University of Pisa

Master Thesis

Dynamic Reduction of Detailed Kinetic Mechanisms and its Coupling with Turbulent Combustion Models

UNIVERSITÀ DI PISA

Candidate:
Francesco D'Ambrosio

Supervisors:
Dr. Ing. Chiara Galletti
Prof. Alessandro Parente

December 2015

Master's Degree in Chemical Engineering

Department of Civil and Industrial Engineering

Acknowledgements

I would like to thank Prof. Chiara Galletti who made my experience in Brussels possible and to Prof. Alessandro Parente who helped me, sustained me during the whole period spent at the ULB and who gave a great contribution to improving my competences, and not only from a professional point of view.
Of course I would like to thank my family, my father, my mother and my little sister, who have never set limits to me and who have helped me, not only from an economical point of view.
Thanks to Andrea, my lifetime friend, with whom I shared both bad and good moments since a long time, before starting the university. Thanks to my flatmate Marco, who was always present when I was in need.
Thanks to my university friends - Bruno (Don Bruno), Giuseppe (Peppe), Carmelo (Melo), Marina, Federica (Fefè), Anna Maria (Nina), Laura, Dario, Saverio (Sav), Vincenzo (Vins), Gianluca (Rizzi), Flavio, Luigi (Gigggi), Giacomo, Picconi - who shared with me every bad and good moment during the last six years, and who helped me to grow.
Thanks to my Brussels friends - Monia, Cristina, Salvatore, Mariano e Alessandro - who made me feel at home and who made unforgettable every single day in Brussels.
Finally, thanks to all other people who stayed close to me during this experience.

Francesco D'Ambrosio
Pisa, December 2015

Ringraziamenti

Ringrazio la professoressa Chiara Galletti per l'aiuto datomi nell'elaborare questa tesi e per avermi dato la possibilità di concludere il mio percorso di studio a Bruxelles. Un enorme grazie va al professor Alessandro Parente il quale mi è stato sempre vicino, mi ha spronato e mi ha fatto crescere dal punto di vista professionale e non solo. Ringrazio anche il professor Alberto Cuoci per l'indispensabile aiuto.
Il mio più grande ringraziamento va alle mie famiglie.
In primis alla mia famiglia vera e propria, mio padre e mia madre che, con sforzo, fatica e dedizione mi hanno reso la persona che sono, e che non hanno mai posto limite, economico e non, alle mie scelte di vita, come quella di intraprendere l'univerità in un posto tanto lontano da casa. A mia sorella Fabiola che mi ha fatto rimanere un po' bambino ma che è stata anche motivo di crescita. Infine a tutti gli altri parenti che mi hanno sempre supportato in questa mia fantastica avventura.
In secondo luogo alle famiglie di Pisa. La prima, formata dai miei coinquilini:Andrea, il mio amico di una vita, un fratello per me, con il quale ho condiviso dolori, fatica, sforzi ma anche gioie e felicità fin da prima che l'università fosse anche solo un'idea e Marco che ringrazio per esserci sempre stato nei momenti di necessità. La seconda è formata dai miei amici universitari che ringrazio per tutto: i momenti di studio, le lezioni, gli esami e i progetti insomma tutti i momenti difficili, noiosi, isterici e mentalmente faticosi ma anche per tutte le pizze, le cene, le Luminare, le serate, i video, le feste insomma tutti i quelli felici, allegri e spensierati. Il mio grazie va a Bruno (Don Bruno), Giuseppe (Peppe), Carmelo (Melo), Marina, Federica (Fefè), Anna Maria (Nina), Laura, Dario, Saverio (Sav), Vincenzo (Vins), Gianluca (Rizzi), Flavio, Luigi (Gigggi), Giacomo e Picconi per aver reso indimenticabile il periodo dell'università.
Infine la mia famiglia di Bruxelles. Monia, Cristina, Salvatore, Mariano e Alessandro grazie ai quali non mi sono mai sentito lontano da casa. Li ringrazio per avermi sempre sostenuto nei momenti di difficoltà e avermi consigliato nei momenti di necessità. Li ringrazio anche per aver reso ogni giorno, dei sei mesi passati insieme, un giorno da ricordare.
Infine ringrazio tutti coloro che non ho citato ma che comunque, in un modo o nell'altro,

mi hanno spronato, hanno tifato per me e mi sono stati vicino lungo tutto questo percorso.

Grazie a tutti

Francesco D'Ambrosio
Pisa, Dicembre 2015

To my family.

Contents

List of Figures

List of Tables

UNIVERSITY OF PISA

Abstract

Chemical Engineering
Department of Civil and Industrial Engineering

Master Thesis in Chemical Engineering

Dynamic Reduction of Detailed Kinetic Mechanisms and its Coupling with Turbulent Combustion Models

by Francesco D'Ambrosio

The description of the combustion phenomena, e.g. turbulence combustion or special fields as pollutants formation, is possible only with the use of large detailed kinetic mechanisms. However, CFD simulations of a practical system that involve complex geometry, heat exchangers, radiation and turbulent flows are prohibitive in industrial applications due to the high computational cost. Therefore, reducing the detailed kinetic mechanisms is necessary in order to obtain alternative schemes (skeletal, reduced or global) that are affordable in time computing and accuracy. Usually the reduction is performed with pre-processing methods using a specific range of operating conditions. During the simulation the characteristics of the flame change, in time and space, while the kinetic scheme is every time the same. This Master Thesis is based on a previous work on the implementation of a reduction method to be used on-the-fly in numerical simulations of laminar reactive flow. In particular the Directed Relation Graph was chosen because of its simplicity and robustness.
The aim of this work is, first to validate this reduction method in the application of a huge kinetic mechanism to a laminar flame, secondly to extend the method to turbulent flame. In order to accomplish that, the Directed Relation Graph is coupled to Eddy Dissipation Concept, Combustion Model for the treatment of the chemical turbulent interactions. The validation of this couple was performed through a series of simple simulations in order to study, also, the sensitivity of the DRG method to the set of variables.

Chapter 1

Introduction

The modelling of combustion processes requires the description of chemical reactions as well as of physical and thermodynamic properties of the gas mixture. A lot of features require the use of detailed kinetic mechanisms in order to properly describe the combustion phenomenon. However, the number of reactions and species increases according to the complexity and the size of the fuel molecule. Things are more complicated if the simulations concern turbulent combustion. Because of the stiffness characterizing the system of non-linear chemical equations, robust numerical algorithms are required.
Several global (one-step two-step) mechanisms are available and widely used for simulations of industrial system, although they are valid only on a specific range of operating conditions and they are not able to describe special features (i.e. soot formation, pollutants, etc) and conditions (i.e. flameless combustion) because they do not allow any analysis of minor species and radicals.
Considering that, the reduction of large kinetic mechanisms to an extent that could limit the loss of informations but at the same time allow the applicability to the modelling of most practical combustion system, is very large appealing. The common approach, in chemistry reductions, consist in performing a sensitivity analysis of the chemical mechanisms for specific conditions of temperature and concentration of species in order to generate skeletal or reduced mechanisms to be used in the simulations. The mechanisms obtained are not updated during the simulations even if the conditions, temperature and concentration of the species, change. The aim of this Master-Thesis is to couple a on-the-fly reduction method for chemistry (DRG) developed during a previous work, with *edcSMOKE*, open solver for turbulent combustion, to validate the model obtained and also to simulate soot precursors formation in laminar flame, using the open laminar solver *laminarSMOKE*, employing a very huge chemistry.
Firstly the DRG algorithms will be added to the edcMOKE, then the solver will be modified in order to make the evaluation of the mass fraction, but only of the important

species, possible. Secondly a Sandia flame D will be simulated with different sets of conditions for DRG in order to validate the coupling. Finally soot precursors formation will be simulated in order to validate the advantage deriving from the use of DRG method with huge chemical kinetic mechanisms.

Chapter 2

Chemical mechanisms reduction

The reduction of the computational time in CFD simulations is one of the most important challenge of the last years in this field. This is due to economical interests, e.g. industrial fields where the coupling between the experimental data and the computational information is possible only if the time for both is of the same order, also to academic interests because of the possibility to simulate complex physical and chemical processes and finally to treat stiff systems. While in some cases the reduction in time computing is applied through editing of the geometry and/or of the mesh, in the combustion field the resolution of the chemistry has a big influence on the simulation time, thus the use of a reduction method has to be taken into account. In fact the combustion models are based on the simultaneous interaction between chemical reactions and physical processes. In a lot of cases only the use of a big kinetic mechanism is able to properly describe a complex case, e.g. it is demonstrated that in flameless combustion the coupling between a turbulence model with a detailed chemistry is necessary [2].
In order to reduce the number of reactions, reduction methods have to be taken into account. A wide variety of reduction methods are shown in literature. DRG (Directed Relation Graph) developed by Lu and Law [3], for example, consists of the generation of a skeletal mechanism using directed relation graph comparing the reaction rate of the species with a threshold value, and subsequent generation of reduced mechanism using computational singular perturbation based on the assumption of quasi-steady-state species . DRGEP (Directed Relation Graph-Error Propagation) (by Pepiot-Desjardins and Pitsch [4]), uses DRG to evaluate the skeletal mechanism, and after its quality is assessed through the magnitude of the errors introduced in the target predictions. The skeletal mechanism taken into account is the one that satisfied a user defined error tolerance [4]. RCCE (Rate Controlled Constrained Equilibrium) is based on the observation that a rate-controlling reaction is equivalent to a passive behaviour, so that the corresponding partial equilibrium state can be calculated by minimizing the appropriate free

energy function [5]. ISAT, that for computational reduction of turbulent combustion simulations is described in [6], is an algorithm for the approximation of non-linear relationship based on multiple linear regressions that are dynamically added as additional information is discovered. It is one of the most powerful and common pre-processing procedure for generation of reduced mechanisms. If high-data fidelity are available from experiment the PCA(Principal Component Analysis) should be applied. PCA ([7]) is able to identify orthogonal variables, which are the best linear representation of the system, to reduce in dimensionality requiring fewer coordinates finally to generate the models using canonical systems. Thanks to these characteristics, manifolds may be determined via PCA, with the principal components forming a new basis to describe the thermochemical state.

All these methods are very powerful but, sometimes, the subsequent reduction in time computing is not enough for a real application, e.g in industrial cases, in CFD simulation. Therefore it is possible to find a solution to this problem by coupling these methods.

In particular Contino et al. [8] developed the TDAC (Tabulation of Dynamic Adaptive Chemistry) method that couples DAC method(Dynamic Adaptive Chemistry) and ISAT. In particular DAC computes a reduced mechanism that is valid for the local thermochemical conditions, i.e. it reduces continuously the mechanism instead of preprocessing it. The ISAT algorithm intends to store the previous information, hence reducing the effect of the mesh(number of cells) whereas the DAC intends to reduce the effect of the mechanism size. Practically DAC uses ISAT to store and map physical and chemical information. Other projects regard the coupling of DRG and PCA, where the PCA should be use to generate a reduced field where DRG is applied, or, vice versa, DRG is used to generate, dynamically, a field where PCA could reduce further the dimension of the system.

In this work DRG(Directed Relation Graph) [3] has been chosen because of its simplicity and robustness, and in particular an on-the-fly version, developed in a previous work. The possibility to dynamically reduce the kinetic mechanism introduces a high level of accuracy with respect to pre-processing methods, and also a reduction of the computing time with respect to the use of the complete kinetic mechanism.

In particular, in this work two different problems have been studied. Both require a detailed chemistry to be properly described. In a first case, the aim was the evaluation of soot precursors (i.e. PAH) thus the kinetic use has been huge, as for the second case the study focused on the coupling of detailed mechanism and turbulence.

Chapter 3

DRG simulations of laminar flames

Soot formation is of a study interest since a long time. Initially the Carbon Black has been studied for its industrial uses as reinforcing agent for rubbers, in the production of automotive tires, painting, petrochemical industry, colour printing ink. Later, due to the harmful influence on human health (e.g. heart attacks, stroke,cardiovascular death and cancer), environmental problems and reduction of combustion efficiency, the research has focused on understanding the mechanisms of formation and growth of soot.
In [9] Longwell shows that soot emission is affected by the propensity of soot particles to absorb polycyclic aromatic hydrocarbons (PAH) onto their surface. PAH can originate from:

- unburned fuel;
- fuel under pyrolysis but that does not burn;
- produced in the flame (if the fuel contains small amounts of PAH or its precursors).

Therefore a great attention has been given to the study of the soot chemistry and its precursors (i.e. PAH).
Soot formation requires an accurate description of the gas-phase chemistry leading to gas-phase PAH formation. A large number of articles show how it is necessary to use a very complex kinetic mechanism to properly simulate the formation of soot precursors in the gas phase. Therefore a huge kinetic mechanism (300 chemical species and 11790 reversible reactions) has been used in order to properly describe the mechanisms of the pyrolis, the partial oxidation and the combustion of Primary Reference Fuels(including

PAH).

An axi-symmetric co-flow non-premixed methane/air flame has been studied. Firstly the computational results obtained have been compared with the experimental data from [1]. After the DRG method has been applied, and the values obtained have been compared with those from the previous simulation, relative to the complete kinetic mechanism.

3.1 Numerical model and Solution Techniques

The burner (see Figure3.1) taken into account is described in [1] [10].

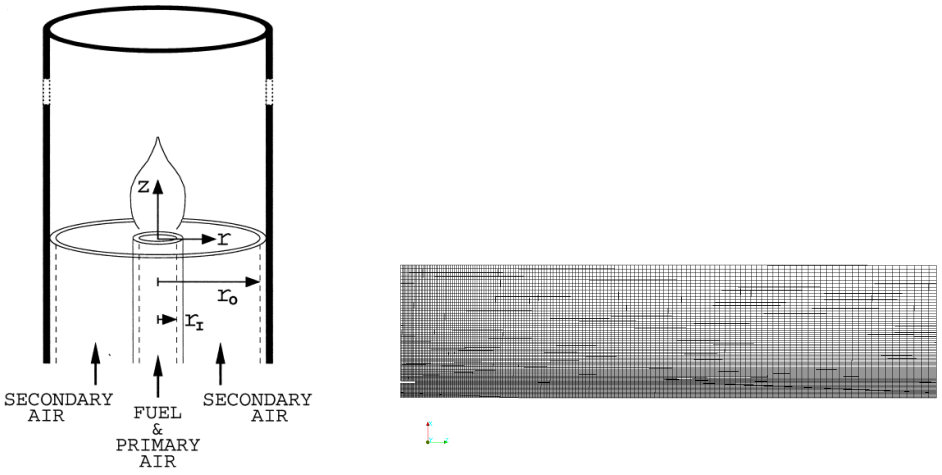

(A) (B)

FIGURE 3.1: (A) Schematic of the burner (B) Computational grid

The central jet radius is $r_I = 5.55$mm, the coflow radius is r_{outer}=50.8mm and the wall thickness of the tube between the two flows is w_{jet}=0.080cm. Finally the length of the chamber is equal to z=20.0cm. The parameters of the two flows, used in the simulations, are reported in Table3.1:

TABLE 3.1: Laminar flame parameters

	ϕ	Q_{CH_4} $(\frac{cm^3}{min})$	Q_{air} $(\frac{cm^3}{min})$	U_z $(\frac{cm}{s})$	X_{CH_4}	X_{O_2}	X_{N_2}	T (K)
Inner jet	∞	330	0	5.67	1.000	0.000	0.000	298
Outer jet	-	0	44000	10.48	0.000	0.232	0.768	298

The velocity across the inner jet consists of a parabolic profile (see [1]) and has been set in the *"U"* file contained in the *"0"* folder:

$$U = U_z \cdot \left(1 - \frac{r_p^2}{r_I^2}\right) \qquad (0 \leq r_p \leq r_I) \tag{3.1}$$

where U_z is the fuel velocity reported in Table3.1. The profile is maximum in the centerline and vanishes on the tube wall.

3.1.1 Numerical Grid

The mesh has been generated with the tool BlockMesh. The final mesh, used for the simulation, has been obtained through a grid independence test.
Three different meshes have been tested. The first one is composed of 6030 cells, the second one of 12198 cells and the last one of 20213 cells. In all the three cases the mesh is finer in the gas inlet zone and grows towards the end of the chamber, either in x and in z directions.
The inlet conditions of the simplify system are the same which have been used for the main simulation(see Table3.1). A parabolic profile has been assumed in the inner jet.
The grid independence process has been applied comparing the results obtained in the simulations, at different axial distances from the inlet zone, to find the coarser grid where the results are independent from the mesh. In order to do that, the radial profiles from 0mm to 200mm, of CH_4, O_2, CO_2, H_2O, U_x and T have been compared along the x-axis for six different distances from the gas inlet. In particular at x=0mm, x=3mm, x=10mm, x=50mm, x=120mm, x=200mm.
Grid independency has been performed with a simplified kinetic mechanism (DRM19, 19species and 84 reactions).

The results obtained are shown in the following section. For sake of clarity, the differences between the three cases, the radial values x reported in the following graphs concern only part of the radius of the burner.

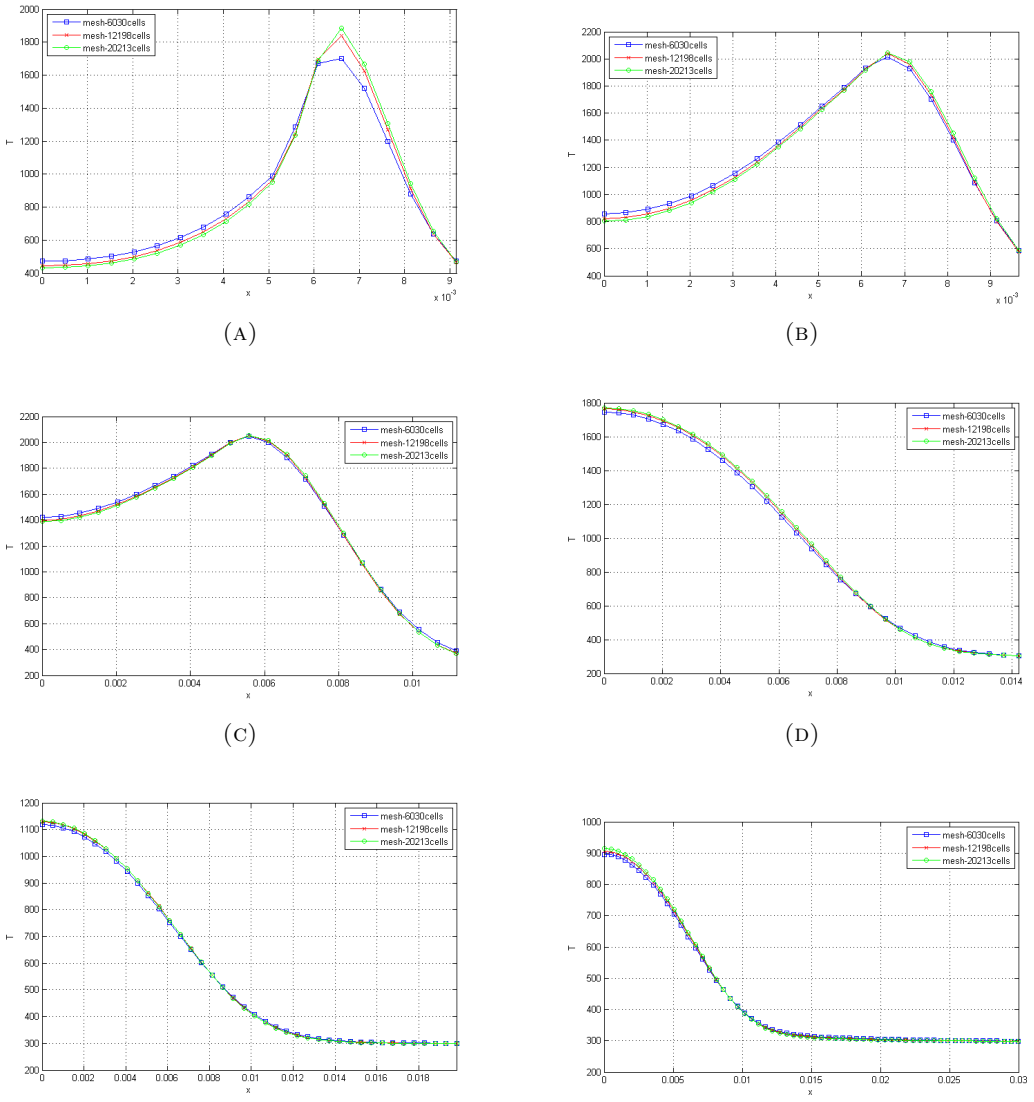

(A) (B)

(C) (D)

(E) (F)

FIGURE 3.2: Radial profiles of temperature (T), in K, at different axial positions (x), in mm, along the axis, obtained for three different grids. The values relative to the three different computational grids are compared at (A) x = 0mm, (B) x = 3mm, (C) x = 10mm, (D) x = 50mm, (E) x = 120mm, (F) x = 200mm

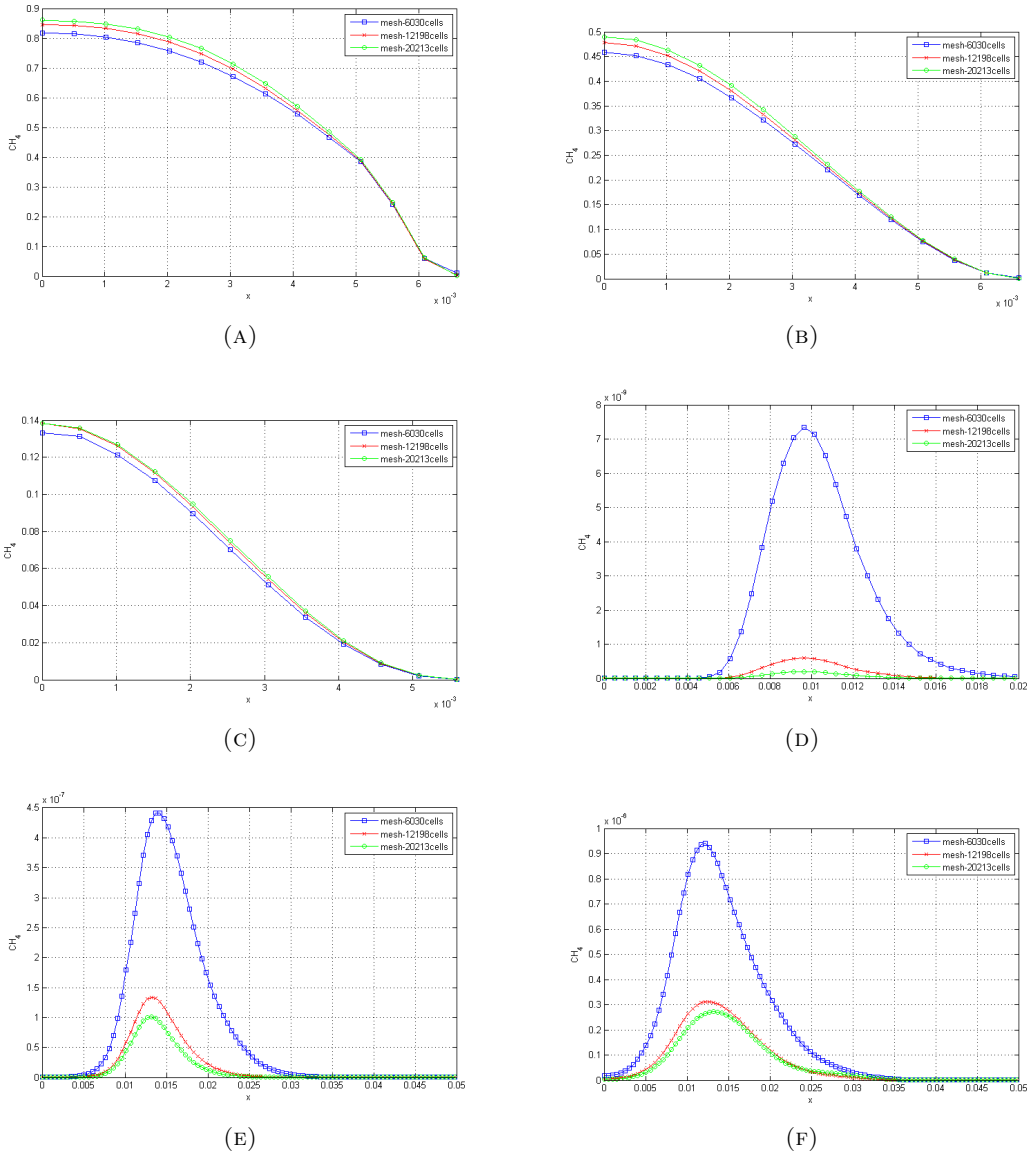

FIGURE 3.3: Radial profiles of CH_4 mole fraction (X_{CH_4}) at different axial positions (x), in mm, along the axis, obtained for three different grids. The values relative to the three different computational grids are compared at (A) x = 0mm, (B) x = 3mm, (C) x = 10mm, (D) x = 50mm, (E) x = 120mm, (F) x = 200mm

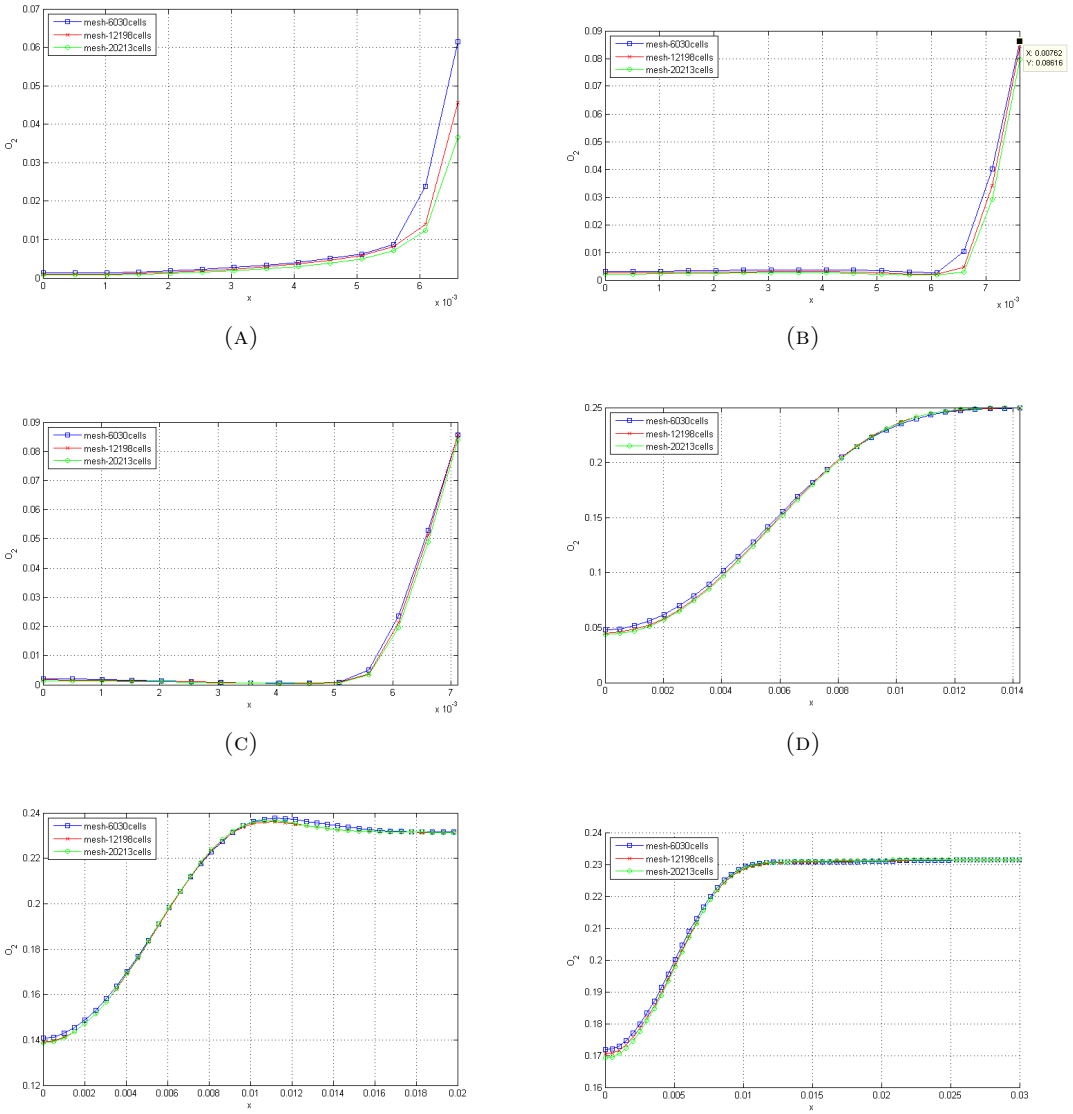

FIGURE 3.4: Radial profiles of O_2 mole fraction (X_{O_2}) at different axial positions (x), in mm, along the axis, obtained for three different grids. The values relative to the three different computational grids are compared at (A) x = 0mm, (B) x = 3mm, (C) x = 10mm, (D) x = 50mm, (E) x = 120mm, (F) x = 200mm

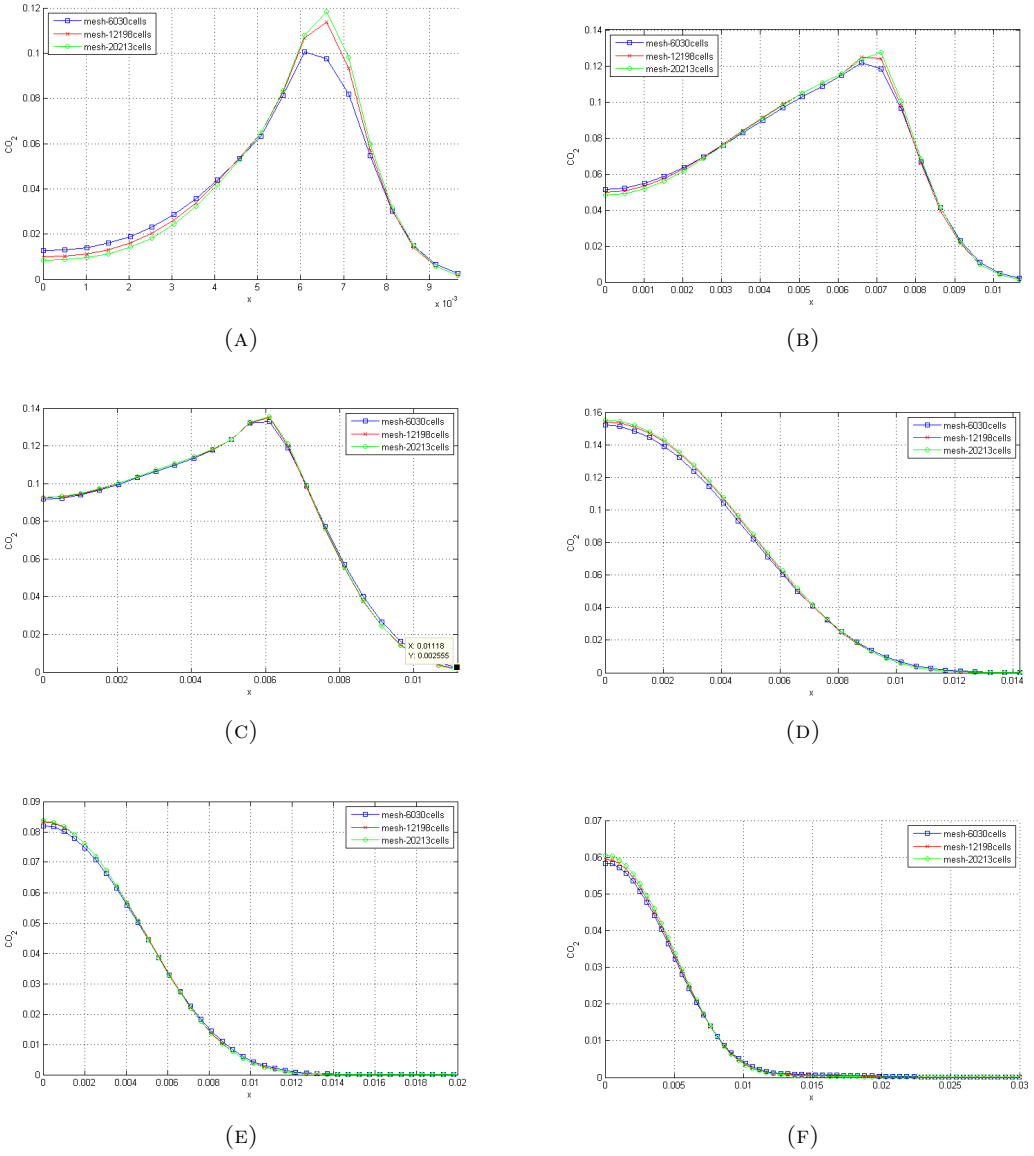

FIGURE 3.5: Radial profiles of CO_2 mole fraction (X_{CO_2}) at different axial positions (x), in mm, along the axis, obtained for three different grids. The values relative to the three different computational grids are compared at (A) x = 0mm, (B) x = 3mm, (C) x = 10mm, (D) x = 50mm, (E) x = 120mm, (F) x = 200mm

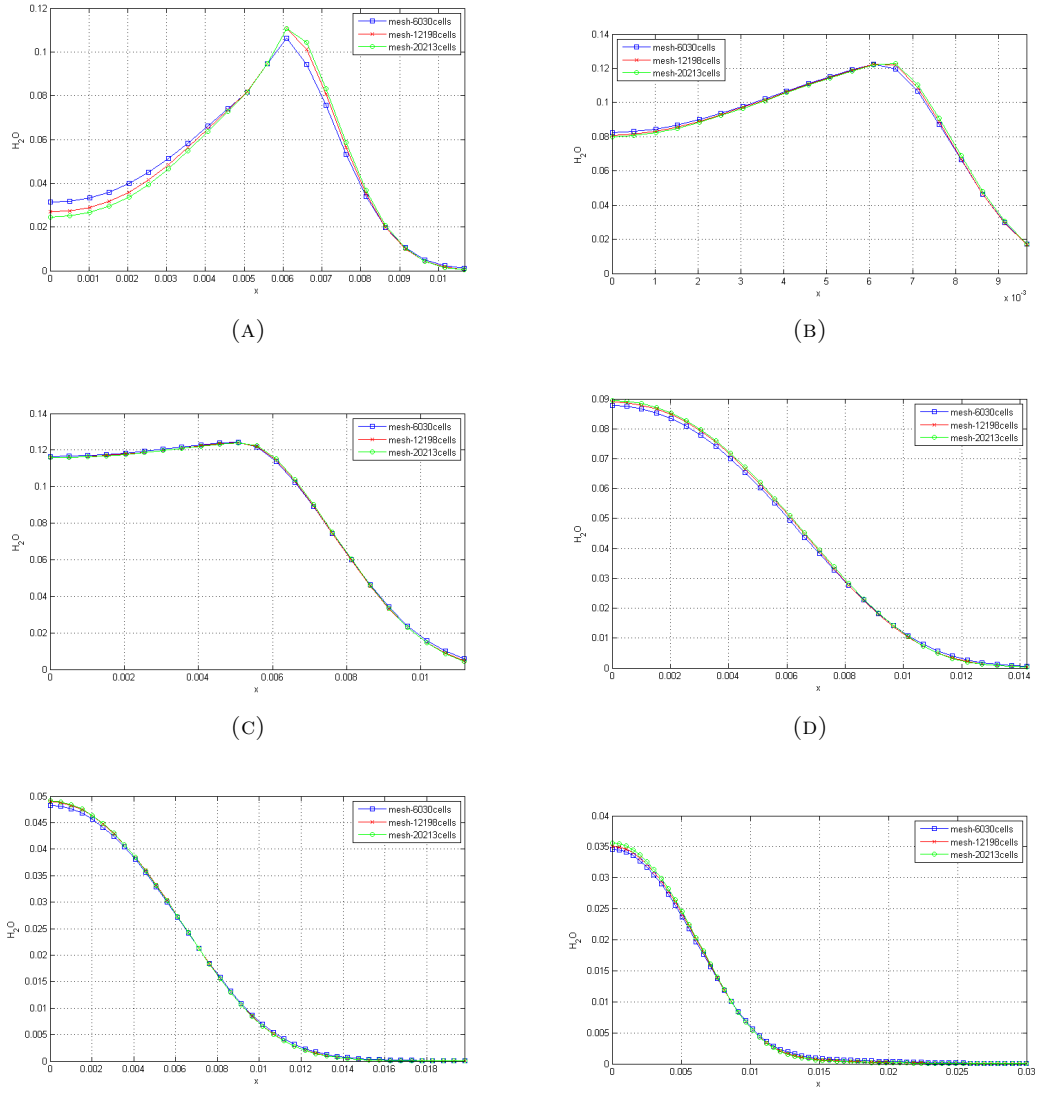

FIGURE 3.6: Radial profiles of H_2O mole fraction (X_{H_2O}) at different axial positions (x), in mm, along the axis, obtained for three different grids. The values relative to the three different computational grids are compared at (A) x = 0mm, (B) x = 3mm, (C) x = 10mm, (D) x = 50mm, (E) x = 120mm, (F) x = 200mm

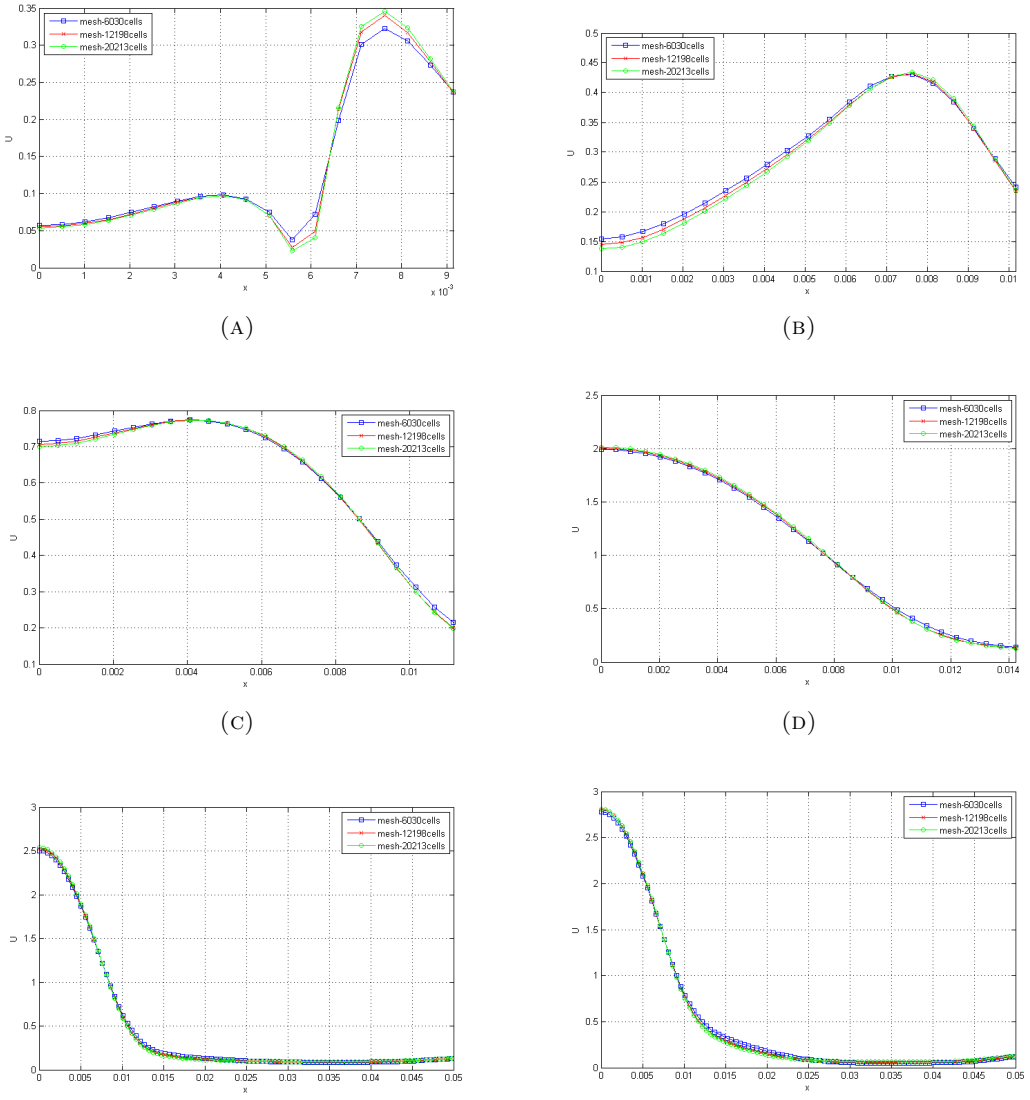

FIGURE 3.7: Radial profiles of axial velocity (U_x), in m/s, at different axial positions (x), in mm, along the axis, obtained for three different grids. The values relative to the three different computational grids are compared at (A) x = 0mm, (B) x = 3mm, (C) x = 10mm, (D) x = 50mm, (E) x = 120mm, (F) x = 200mm

The results obtained with the mesh 12198 and 20213 are very similar, for each axial distance and for each case, in spite of the cells are double. Therefore the mesh 12198 has been chosen for the main simulation.

3.1.2 Physical Models

The simulations have been performed with the open source solver *"laminarSMOKE"* ([11]) and in particular with the steady state solver *"laminarSimpleSMOKE"*, which is based on the OpenSMOKE++ numerical framework [12].
All the calculations have been performed on 8CPU. The decomposition of the mesh, set in the *"decomposeParDict"* file present in *"system"* folder, has been performed through the *"scotch"* option.
The kinetic mechanism chosen for the simulation is the POLIMI_PRF_PAH_LT_1412 ("Primary Reference Fuels (PFR) + PAH mechanism") consisting of 300 species and 11790 reactions developed by the CRECK Modeling Group , from Politecnico di Milano, and available at [13]. This kinetic is huge and it takes a lot of time to come to convergence. Moreover, starting the simulations with a complex kinetic mechanism from the beginning is not the fastest and the most robust method to obtain the convergence. Therefore the simulations have been split in several steps.
In order to generate initial conditions that could make it easier the convergence of simulations, the coarser mesh (6030 cells) has been used during the first step and also a set of simpler kinetic mechanisms which are shown in Table3.2.

TABLE 3.2: Set of kinetic mechanisms used for the simulations

Kinetic Mechanism	Description	Reference
DRM19	19 species, 84 reactions	[14]
GRI-Mech3.0	53 species,325 reactions	[15]
POLIMI_C1C3HT	84 species, 1698 reactions	[16]
POLIMI_PAH_HT	176 species, 6067 reactions	[17]

The DRM19 has been used to start the simulation. The initial conditions are those above. Once a convergence, the results from DRM19 are used as initial values for the same simulation with GRI-Mech3.0. This procedure has been repeated for POLIMI_C1C3HT and POLIMI_PAH_HT. The discretization method *"upwind"* has been used for this step. Finally to light the flame, a spark ignition has been simulated in proximity of the exit of the methane during the first time step of the simulation with DRM19. The unsteady solver *"laminarPimpleSMOKE"* has also been used at the same time.

With the results obtained from the last simulation, the POLIMI_PRF_PAH_LT_1412 has been applied before in the coarse mesh and, once a convergence, the fields (T,P,Y_i,..)

have been mapped in the fine mesh (12198 cells) through the command *"mapFields"* from OpenFOAM.
The convergence has been reached before with first order discretization (*"upwind"*), and after with second order discretization (*"limitedLinear"*).
The DRG has to be set in the *"solverOption"* file, contained in the *"costant"* folder.
The setting required a minimum temperature value (minTemperature), a vector of temperatures (of size 2 in this case) and a threshold value, ϵ, that is function of temperature, so it is possible to set two different values of ϵ, one is used below the lowest temperature and another value, smaller than the first one, that is used in the reaction zone.
The values relative to the DRG setting are reported in Table3.3. The key set of species has been taken into account on the basis of the studies by Contino et al. [8] about comparative analysis of kinetic mechanism reduction methods.

DRG	
minT	280
temperature	700 4000
epsilon	1e-1 1e-2
species	CH_4 HO_2 CO

Table 3.3: DRG-setting

3.2 Results

3.2.1 Complete mechanism

In the following section the results obtained from the simulations are compared with the experimental data from [1]. In all the following figures, the nondimensional axial position z/H_T is plotted on the abscissa, where z is the dimensional axial position and H_T is the distance, in the centerline, at which the maximum temperature $T_{max,C}$ occurs. The mole fractions of the major species and the temperature profiles are shown in Figure 3.8.

The **temperature** profiles, Figure3.8a, show that the computational trend is the same as experimental results. In general, in the hottest area, the computational values are higher than the corresponding experimental ones (e.g. the difference between the maximum temperature is 45K). In first part of the burner the experimental data are higher than the computational ones. This behaviour partly results from the experimental uncertainties reported in [1], but also from the thermal boundary condition at the burner surface. Both the maximum values of temperature are positioned close to the same distance of $z/H_T \simeq 1$.

Figure3.8b shows the trend of **CH_4 mole fractions**. In this case the mole fractions from the experimental data are much lower than the computational ones. This behaviour is probably due to wrong calibration of Ar in the CH_4 used for the experimental campaign. However, the authors report an absolute uncertainty of 30% relative to the experimental data.

Mole fractions of O_2 along the centerline are illustrated in Figure3.8c. As mentioned for the CH_4, the computational trend underestimates the O_2 concentration. Anyway the experimental data are conditioned by a not exact calibration of Ar and also some O_2 is entrained through the weak flame front near the burner (see [1]). Elsewhere, both the results are in good agreement about the distance at which the O_2 first disappears ($z/H_T \simeq 0.55$) and after reappears ($z/H_T \simeq 0.9$).

As with H_2O mole fractions, the results of **CO_2**, Figure3.8b, show a marked quantitative difference but a similar qualitative behaviour. The Figure3.8e shows the **H_2O mole fractions**. The experimental values have been multiplied through by a scale factor unknown that makes it impossible a quantitative comparison but qualitatively the shapes are similar. Finally the mole fractions of C_2H_2 along the centerline are shown in the Figure 3.8f. Computational and experimental agree well and the shapes are similar.

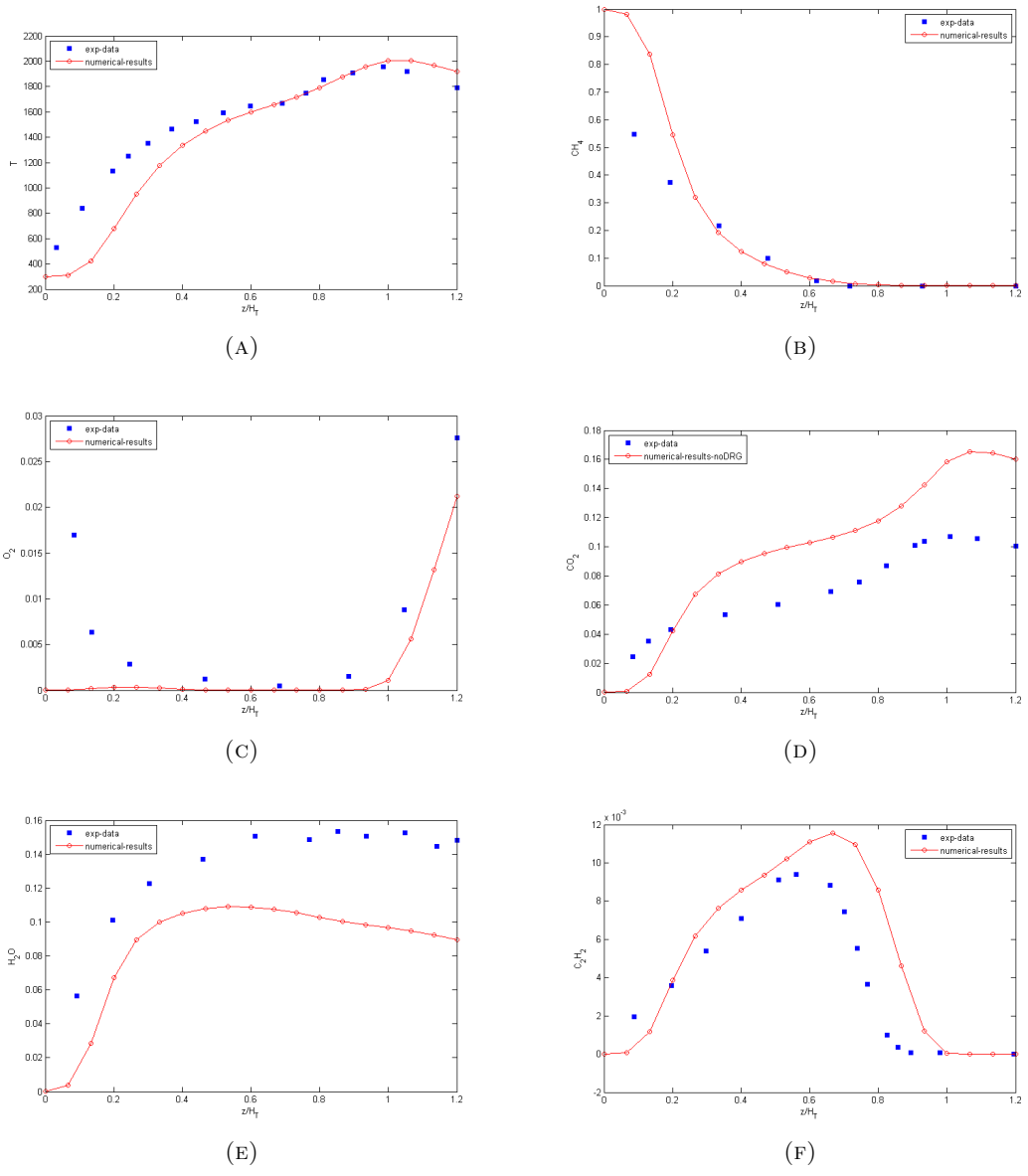

FIGURE 3.8: Profile of major species mole fractions and temperature (in K) along the flame centerline as function of nondimensional axial position z/H_T. Computational results are compared with the experimental results ([1]), i.e. (A) Temperature, (B) X_{CH_4}, (C) X_{O_2}, (D) X_{CO_2}, (E) X_{H_2O}, (F) $X_{C_2H_2}$

3.2.2 DRG

In this section the trends of the temperature and of the mole fractions of the major species along the flame centerline are reported. The computational results of the previous section have been compared with those obtained with DRG method.
Figure3.9 shows the results of the simulation. The **temperature** values from simulation with DRG, Figure3.9a, are in good agreement with the results of the simulation with the complete kinetic scheme. The **CH_4 mole fractions** along the centerline are shown in Figure3.9b. As for the temperature, the two shapes are overlapped. This results are in full agreement with the expectation because CH_4 is one of the species of the key set of DRG. **Mole fractions of O_2** are illustrated in Figure3.9c. Also in this case the two curves have the same behaviour for the whole length of the burner although, in the last part, the DRG overestimates the O_2 mole fraction of 15% to the simulation with complete kinetic mechanism but it is closer to the experimental value. This may be due to the key set of species of DRG that does not include O_2. The results, along the centerline, relative to the main products, **H_2O and** $mathbfCO_2$, are reported in Figure3.9d and Figure3.9e respectively. In both cases the reduction method gives values that are in good agreement with the complete kinetic ones. Because of the high reactive of OH with CH_4 and H_2, the Figure3.9f shows that the production of OH occurs in the region $0.7 \leq z/H_T \leq 1.2$ where the molar fraction of CH_4 decreases. The peak occurs, in both cases, to $1 \leq z/H_T \leq 1.1$ and DRG overestimates the values of 5%. More generally, the curve is shifted towards the inlet of the combustion chamber. Finally the **mole fractions of the BIN1A anb BIN1B**, along the centerline, are reported in Figure3.9g and in Figure3.9h. This two species represent groups of soot precursors that have been studied in order to compare soot formation. In both cases the simulation with the reduction method underestimates the peak of mole fraction, of 5% for the BIN1A and of 10% for BIN1B, but in all the other points results agree with the complete kinetic simulation. Finally the **trend of the number of important species and the trend of the number of important reactions** are showed in Figure3.10a and in Figure3.10b. As expected, the area where the DRG takes into account a bigger number of species and reactions is the hottest one, where the combustion takes place.

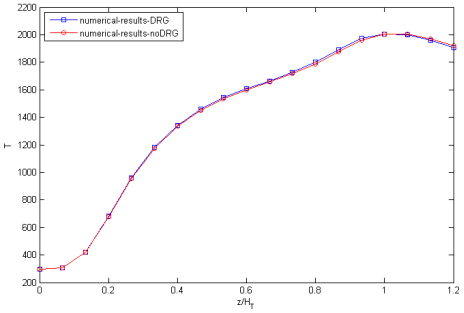

(A) *Temperature*

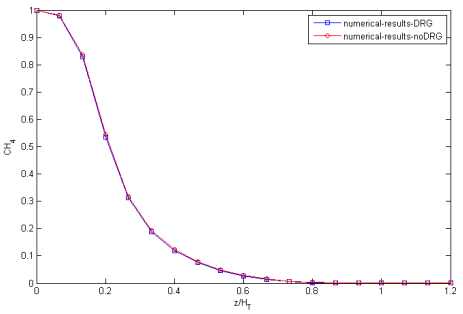

(B) CH_4 *mole fractions* X_{CH_4}

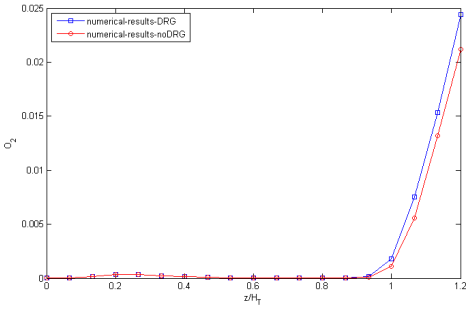

(C) O_2 *mole fractions* X_{O_2}

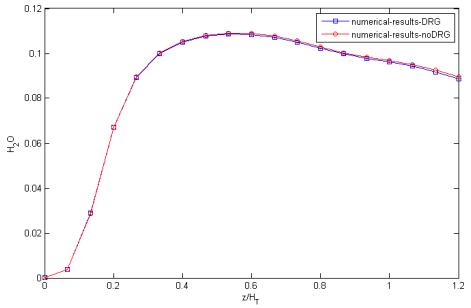

(D) H_2O *mole fractions* X_{H_2O}

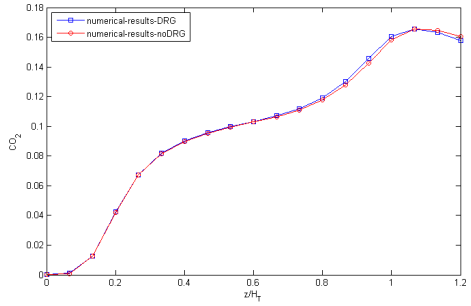

(E) CO_2 *mole fractions* X_{CO_2}

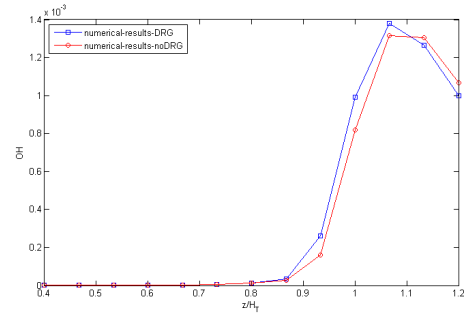

(F) OH *mole fractions* X_{OH}

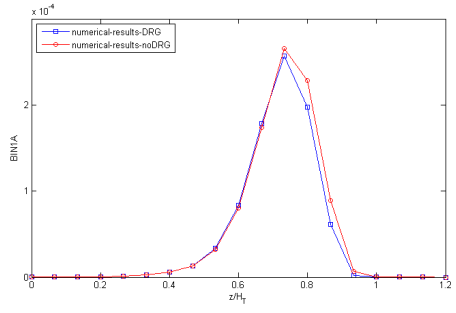

(G) $BIN1A$ *mole fractions* X_{BIN1A}

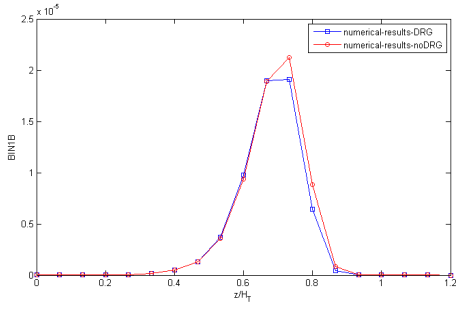

(H) $BIN1B$ *mole fractions* X_{BIN1B}

FIGURE 3.9: Profile of major species mole fractions and temperature (in K) along the flame centerline as function of nondimensional axial position z/H_T. The results of the DRG analysis are compared with the numerical simulation without the reduction method for kinetic mechanism, i.e. (A) Temperature, (B) X_{CH_4}, (C) X_{O_2}, (D) X_{CO_2}, (E) X_{H_2O}, (F) $X_{C_2H_2}$

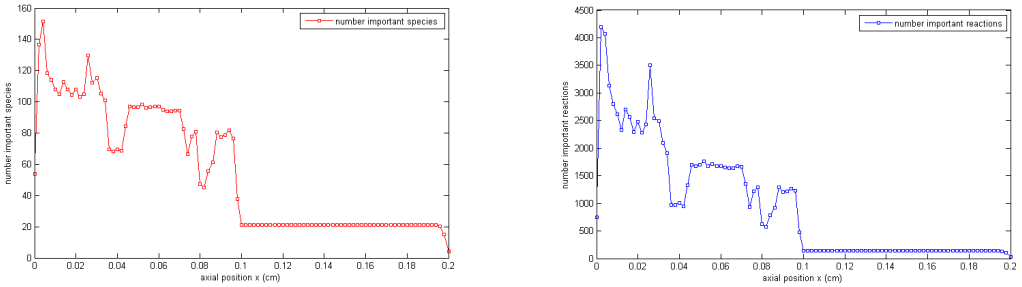

(A) (B)

FIGURE 3.10: Profile of important species (A) and important reactions (B) along the flame centerline as function of nondimensional axial position z/H_T.

3.2.3 Conclusion

The simulations have been run in parallel with the same number of processors. The Table3.4 shows the time to convergence of the two different cases in order to compare the complete kinetic mechanism case and the DRG case.

Case	Time [hr]
Complete Kinetic	≈ 165
DRG	≈ 89

TABLE 3.4: Comparison of time to convergence between the simulation with complete kinetic mechanism and the case with DRG

As expected, the DRG method reduces the CPU time and predicts almost the same results of the case with the complete detailed mechanism.

The aim of this work, regarding the laminar flame simulations, has been to use a very huge kinetic mechanism in order to properly describe a special feature such as soot precursor formation. Indeed these species, grouped under the name BIN in the kinetic mechanism used for the simulation, are compared for the two cases performed (see 3.9g and 3.9h) showing a very good agreement of the DRG results. Moreover the computational time saved, using DRG, is equal to 46% less. Therefore both accuracy and computational time confirm the DRG as a good reduction method to run on-the-fly for CPU time saving.

Finally, in Appendix A the contour plots of the different cases are reported. In particular, those relative to the number of important species and number of important reactions, show clearly where DRG works. Indeed the combustion area is characterized by a big number of species, therefore reactions, taken into account while the non-reacting zones show an activity close to zero.

Chapter 4

Coupling DRG to EDC combustion model

In the majority of industrial applications , (e.g. internal combustion, burners, furnaces) the combustion is characterized by turbulent flow conditions. Turbulence increases the mixing between fuel and oxidizer and enhances the combustion. As a matter of fact, it increases the mass consumption rate of the reactants to values much greater than those obtained with laminar flames. In extreme case, when the turbulence is such as to perfectly mix the fluid present in a combustion chamber, the temperature field becomes homogeneous in each point, the maximum temperature value and the production of pollutants decrease considerably with consequent benefits on the environmental impact. However the numerical simulation of a turbulent reactive flow represents one of the most complicating task in CFD simulations. The principal reasons are:

- **Turbulence** is a very complex phenomenon that involves different time-scales and space-scales. The simulations of a turbulent flow require the choice of one of the available methods (e.g. $k-\epsilon$, $k-\omega$), that described only partially the real nature of a turbulent phenomenon.
- **Chemical reactions** in a combustion phenomena consist in hundreds of species and thousand of reactions. A CFD simulation, which should take into account a complex kinetic mechanism, may require calculation time that is too long for a real application even just for laminar flame.
- **The interactions between chemistry and turbulence** further complicate the problem, because the heat released during the reactions modifies the local physical properties(i.e. density, viscosity) and because, if the turbulence is too strong it

can extinguish the reactions, and if it is too weak reactants may not mix enough to start to react.

Therefore evaluating the most important aspect is one of the first step to correctly simulate a flame. The interaction between turbulence and chemistry may be evaluated through the analysis of the Damköhler number, which relates the characteristic fluid scale and the chemical time scale:

$$Da = \frac{\tau_T}{\tau_C} = \frac{l/u'}{\delta_r/S_L} \tag{4.1}$$

where l is the turbulent length scale, u' is the turbulent intensity, δ_r the flame thickness and S_L the laminar flame speed. Large Damköhler values are typical of conventional flames, it indicates that mixing is time controlling while small Damköhler number corresponds to chemical control then the turbulence mixes slowly reactants and products. For example, in flameless condition, Da is approximately equal to unity [18] [19], implying that simulations have to take into account both chemistry and mixing aspect.

In order to obtain good results from simulations of turbulent flames, appropriate combustion models must be taken into account.
Indeed the objective if turbulent combustion modelling i to provide closure for the unknown quantities in the Navier-Stoke equations. In particular, the closure i relative to the following terms:

- **Reynold stresses $\widetilde{\mathbf{u_j''}\mathbf{u_i''}}$**. The closure is done in most of studies using the Boussinesq hypothesis 4.2, which assume for the Reynolds stresses the same dependency assumed for the viscous tensor given by the Newton law:

$$\widetilde{\overline{\rho} u_j'' u_i''} = -\mu_t \left(\frac{\partial \tilde{u}_i}{\partial x_j} + \frac{\partial \tilde{u}_j}{\partial x_i} - \frac{2}{3}\delta_{ij} \frac{\partial \tilde{u}_k}{\partial x_k} \right) + \frac{2}{3}\overline{\rho} k \tag{4.2}$$

  where μ_t i the turbulent viscosity, k is the kinetic energy, and δ_{ij} i the Kronecker symbol. Therefore the role of the turbulent model is to provide an estimation of the turbulent viscosity. The $k-\epsilon$ model is one of the most popular because of it simplicity. Popular turbulence models such as $k-\epsilon$ assume isotropic turbulence but practical flow often show strong anisotropic behaviour. Relaxing the Boussinesq hypothesis and solving transports equations for the Reynolds stresses , these phenomena can be incorporated. This leads to the so called Reynolds Stress Models (RSM), which requires six additional transport equations.

- **Species, $\overline{\rho}\widetilde{\mathbf{u_j''Y_k''}}$, and enthalpy, $\overline{\rho}\widetilde{\mathbf{u_j''h_t''}}$ turbulent fluxes.** They are usually closed using a gradient assumption:

$$-\overline{\rho}\widetilde{u_j''Y_k''} = \frac{\mu_t}{Sc_{kt}}\frac{\partial \tilde{Y_k}}{\partial x_j} \tag{4.3}$$

$$-\overline{\rho}\widetilde{u_j''h_t''} = \frac{\mu_t}{Pr_{kt}}\frac{\partial \tilde{h_t}}{\partial x_j} \tag{4.4}$$

  where Sc_{kt} is the turbulent Schmidt number and Pr_{kt} is the turbulent Prandtl number.

- **Species mean reactions rates, $\overline{\dot{\omega}}_{\mathbf{k}}$.** Turbulent combustion modelling focused on developing closure models for such terms.
  A combustion process can be described in term of M elementary reactions involving N species:

$$\sum_{k=1}^{N} \nu_{k,j}^{'} M_k = \sum_{k=1}^{N} \nu_{k,j}^{''} M_k \quad j = 1, 2, ..., M \tag{4.5}$$

where $\nu_{k,j}^{'}$ and $\nu_{k,j}^{''}$ are the molar stoichiometric coefficients of species k in reaction j and M_k is the symbol for species k.
The net mass reaction rate for species k is given by:

$$\dot{\omega}_k = \sum j = 1^M \dot{\omega}_{kj} = W_k \sum j = 1^M (\nu_{k,j}^{''} - \nu_{k,j}^{'}) Q_j \tag{4.6}$$

where W_k i the molecular weight of species k and Q_j is the rate of progress for reaction j and is function of the kinetic constants k_{fj} and k_{rj}.

Eddy Dissipation Concept is one of the approaches for the estimation of the mean species reaction rates, $\dot{\omega}_k$, in turbulent flames.

4.1 EDC Combustion Model

Turbulent combustion simulations could be performed with different models (ED, ED/FR, EDC, etc.) according with physical and chemical systems.
This work has focused on the Eddy Dissipation Concept (EDC), that is an extension of the Eddy Dissipation Model, developed by Magnussen [20], [21], [22]. EDC model has been chosen because, as demonstrated in various studies [2], it ensures the best results in

applications requiring both turbulent models and detailed kinetic mechanisms. According with this model, the chemical reactions take place thanks to the molecular mixing and when the temperature is sufficiently high. In addition the processes that happen at the microscale, as molecular mixing and dissipation of energy into heat(see after), are intermittent, non-homogeneous and localized in small fractions of the volume called fine structures, where the processes above take place. Therefore it is possible to study this part of volume as small reactors by the fluid with mean properties. In order to be able to study the evolution of reactions within the fine structure, it is necessary to know the volume, the reacting fraction of the fine structure and the rate of mass transfer from mean flow to fine structure.

4.1.1 EDC Theory

The energy in a turbulent flow is stored in the big vortices and transferred from these to the neighbours (turbulent energy cascade [20]). Starting from the big, anisotropic eddies, the kinetic energy is transferred until the smallest scale, the Kolmogorov scale, where the eddies become isotropic, and finally dissipated in heat by the molecular forces(friction). The energy transferred is described by the turbulent kinetic energy ω while the energy dissipated is evaluated through the turbulent dissipation rate ϵ that is equal to the sum of the dissipation rates q.
The turbulent flow could be described by the turbulence velocity, u and the turbulent length, l. The turbulent eddy velocity, ν_t links these two quantities:

$$\nu_t = u \cdot l \tag{4.7}$$

The transfer of energy is described by the step-wise energy cascade:

- The 1^{st} **structure level** is characterized by the turbulent velocity u', and the turbulent length l' (see above). The production of turbulent kinetic energy in this step is equal to:

$$\omega' = \frac{u'}{l'} \quad where \quad u' = \left(\frac{2}{3} \cdot k\right)^{\frac{1}{2}} \tag{4.8}$$

  where k is the turbulent energy.

  At this level it is represented all the whole spectrum of turbulence.

- The 2^{nd} **level** represents, only, a part of the spectrum. It is characterized by u'',l''. The vorticity and the dissipation are equal to:

$$\begin{aligned} \omega'' &= 2 \cdot omega'; \\ \epsilon &= q' + w''; \end{aligned} \tag{4.9}$$

The transfer from the first to the second level, w'', is modelled to be proportional to the square of the characteristic fluctuation at 2^{nd} level, u'' and proportional to the strain rate at 1^{st} level while the dissipation, at 2^{nd} level is assumed to be proportional to viscosity and to strain rate. In particular:

- The energy transferred between the 1^{st} and the second level is:

$$\begin{aligned} w'' &= \frac{3}{2} \cdot C_{D1} \cdot 2 \cdot u''^2 \cdot \omega' \\ &= \frac{3}{2} \cdot C_{D1} \cdot u''^2 \cdot 2 \cdot \frac{\omega''}{2} \\ &= \frac{3}{2} \cdot C_{D1} \cdot \frac{u''^3}{l''} \end{aligned} \tag{4.10}$$

- The mechanical energy transformed in heat energy in the 2^{nd} level is equal to:

$$q'' = C_{D2} \cdot \nu \cdot \omega''^2 \tag{4.11}$$

- The transfer from 2^{nd} **to** 3^{rd} level is equal to previous levels where w' is equal to w", u' to u" etc.
- The **last level** is the **fine structure level** characterized by u^*, l^* and ω^*, that are of the same order of magnitude of the Kolmogorov scales.

  At this level almost the 3/4 **of the energy is dissipated**.

In the same way, the expression above can be developed for each level, starting from the 1^{st} to the n^{th} level, where they are equal to:

$$w_n = \frac{3}{2} \cdot C_{D1} \cdot \omega_n u_n^2 \tag{4.12}$$

$$q_n = C_{D2} \cdot \nu \omega_n^2 \tag{4.13}$$

In the equation above, Eq. 4.12 4.13, C_{D1} is equal to 0.135 and C_{D2} to 0.5. They are the values used by Magnussen [20] in the cascade model and they are evaluated as later described.
By definition the turbulent dissipation rate, ϵ is equal to the sum of all the dissipation terms:

$$
\begin{aligned}
&\epsilon = q* + q_n + q_{n-1} + ... + q' = \\
&= C_{D2} \cdot \nu \cdot {\omega^*}^2 + C_{D2} \cdot \nu \cdot \omega_n^2 + ... = \\
&\textit{considering Eq.}4.9 \\
&= C_{D2} \cdot \nu \cdot {\omega^*}^2 + C_{D2} \cdot \nu \cdot \frac{{\omega^*}^2}{4} + ... = \\
&= q^* \sum_{k=0}^{\infty} \frac{1}{2^{2k}} = \frac{4}{3} \cdot q^* = \frac{4}{3} \cdot C_{D2} \cdot \nu \cdot {\omega^*}^2 \\
&\textit{because } \sum_{k=0}^{\infty} = 1 + \frac{1}{4} + \frac{1}{16} + ... \simeq 1 + \frac{1}{3} = \frac{4}{3}
\end{aligned}
\tag{4.14}
$$

In the last level of energy cascade, all the mechanical energy transferred from the previous level is transformed in heat energy, $q^* = w^*$, therefore:

$$
\begin{aligned}
&\epsilon = \frac{4}{3} \cdot q^* = \frac{4}{3} \cdot w^* = \\
&\textit{considering Eq.}4.12 \\
&= \frac{4}{3} \cdot \frac{3}{2} \cdot C_{D1} \cdot {u^*}^2 \cdot \omega^* = 2 \cdot C_{D1} \cdot \frac{{u^*}^3}{l^*}
\end{aligned}
\tag{4.15}
$$

From the Eqs. 4.14 and 4.15 it is possible to derive the characteristic scales for the fine structure:

$$
\begin{aligned}
&l^* = \frac{2}{3} \cdot \frac{C_{D2}}{C_{D1}} \cdot \nu \cdot \frac{1}{u^*} \quad \textit{from Eq.}4.14, \quad u^* = \left(\frac{3 \cdot \epsilon \cdot {l^*}^2}{4 \cdot \nu \cdot C_{D2}} \right)^{1/2}; \\
&l^* = \frac{2}{3} \cdot \left(\frac{3 \cdot {C_{D2}}^3}{C_{D1}^2} \right)^{1/4} \cdot \left(\frac{\nu^3}{\epsilon} \right)^{1/4}
\end{aligned}
\tag{4.16}
$$

$$
\begin{aligned}
&u^* = \frac{2}{3} \cdot \frac{C_{D2}}{C_{D1}} \cdot \nu \cdot \frac{1}{l^*} \quad \textit{from Eq.}4.14, \quad l^* = \left(\frac{4 \cdot C_{D2} \cdot \nu \cdot {u^*}^2}{3 \cdot \epsilon} \right)^{1/2}; \\
&u^* = \left(\frac{C_{D2}}{3 \cdot C_{D1}^2} \right)^{1/4} \cdot (\nu \cdot \epsilon)^{1/4}
\end{aligned}
\tag{4.17}
$$

At the highest energy levels, the viscous dissipation is not important; therefore the energy dissipation is:

$$\epsilon = q' + w'' \simeq w'' = \frac{3}{2} \cdot C_{D1} \cdot \frac{u''^3}{l''} \tag{4.18}$$

Following the previous equation, the turbulent viscosity $\nu_T = u' \cdot l'$ can be expressed as follows:

$$\nu_T = \frac{3}{2} \cdot C_{D1} \cdot \frac{u'^3}{\epsilon} = \frac{2}{3} \cdot C_{D1} \cdot \frac{k^2}{\epsilon} \tag{4.19}$$

Then, $2/3 \cdot C_{D1}$ corresponds to the constant $C_\mu = 0.09$ used in $k - \epsilon$ model.

This means that the most important processes that happen during combustion can be studied at this level, considering only the mass transfer between mean flow and the fine structure.

In order to be able to treat the reactions occurring within this space, it is necessary to know the mass fractions occupied by the fine structure. It can be expressed as:

$$\begin{aligned} \gamma^* &= \left(\frac{u^*}{u'}\right)^3 \\ &\textit{from Eq.4.17 and from the definition of } u'; \\ \gamma^* &= \left(\frac{3 \cdot C_{D2}}{4 \cdot C_{D1}^2}\right)^{\frac{3}{4}} \cdot \left(\frac{\nu \cdot \epsilon}{k^2}\right)^{\frac{3}{4}}; \end{aligned} \tag{4.20}$$

In 2005 this equation has been modified by Magnussen, [21], as follows:

$$\gamma^* = \left(\frac{u^*}{u'}\right)^2 = \left(\frac{3 \cdot C_{D2}}{4 \cdot C_{D1}^2}\right)^{\frac{1}{2}} \cdot \left(\frac{\nu \cdot \epsilon}{k^2}\right)^{\frac{1}{2}}; \tag{4.21}$$

basing on the assumption that the fine structures are localized in nearly constant energy regions where the turbulence kinetic energy can be characterized by u'^2.
The mass fraction γ^* is defined because it is necessary to know the reaction mass fraction and the mass transfer between the fine structures and the surrounding flow.
Assuming that the fine structure are cylindrical, with diameter equal to the characteristic length l^* and height equal to h, the mass flow across their boundary is given by:

$$\dot{M}^* = \rho^* \cdot u^* \cdot A^* = \rho^* \cdot u^* \cdot \frac{\pi \cdot l^* \cdot h}{2}. \tag{4.22}$$

The mass transfer, per unit of mass is:

$$\dot{m}^* = \frac{\dot{M}^*}{\rho^* \cdot V^*} = \frac{\rho^* \cdot u^* \cdot \frac{\pi \cdot l^* \cdot h}{2}}{\frac{\rho^* \cdot \pi \cdot l^{*2} \cdot h}{4}} = 2 \cdot \frac{u^*}{l^*} \tag{4.23}$$

using Eqs. 4.16 and 4.17, $\dot{m}^*$ is also equal to:

$$\dot{m}^* = \left(\frac{3}{C_{D2}}\right)^{\frac{1}{2}} \cdot \left(\frac{\epsilon}{\nu}\right)^{\frac{1}{2}} \tag{4.24}$$

The inverse of this quantity, $\tau^* = 1/\dot{m}^*$, is regarded as the characteristic time-scale of the fine structures so it is the fluid-dynamic time scale for the reactions.

Finally the mass transfer between the fine structures and the surrounding fluid is equal to:

$$\dot{m} = \dot{m}^* \cdot \gamma^* \tag{4.25}$$

and it can be interpreted as the mean rate of the molecular mixing.

Once defined the relations that described the smallest scale in a turbulent system, the mass transfer in the fine structures and between the smallest scale and the surrounding fluid, it is time to describe the reaction rate of a species i.
Actually the fine structures are formed, internally, by sub-fine structures which have formation and dissipation timescale smaller than the Kolmogorov timescale. This means that the mixing within the fine structure is fast enough to hypothesize that this structure are perfectly mixed. Therefore they are treated as perfect stirred reactors (PSR). Therefore the reaction rate is given by:

$$\bar{R}_i^* = -\bar{\rho}^* \cdot \dot{m}^* \cdot \left(Y_i^0 - Y_i^*\right) \tag{4.26}$$

The mean net mass transfer rate $\bar{R}_i$ between the surrounding fluid and the reacting fraction, χ, of the fine structure can be expressed as follows:

$$\bar{R}_i = -\bar{\rho} \cdot \dot{m} \cdot \chi \cdot \left(Y_i^0 - Y_i^*\right) = -\frac{\bar{\rho} \cdot \dot{m} \cdot \chi}{1 - \gamma^* \cdot \chi} \cdot \left(\tilde{Y}_i - Y_i^*\right) \tag{4.27}$$

In the Eq. 4.27, "0" refers to the fluid and " $*$ " to the fine structure. The $\tilde{Y}_i$, necessary for CFD calculations, is a mean mass fraction between fine structure and surrounding fluid. It is defined as:

$$\tilde{Y}_i = Y_i^* \cdot \gamma^* \cdot \chi + Y_i^0 \cdot (1 - \gamma^* \cdot \chi) \tag{4.28}$$

On the basis of these theoretical concepts, the DRG method has been coupled to the EDC solver.

4.1.2 EDC in OpenFOAM

"edcSMOKE" is a solver for OpenFOAM capable of using detailed chemical reaction mechanisms. This is possible because of the use of the EDC as combustion model. The standard solver of OpenFOAM for turbulent reacting flow, *"reactingFoam"*, is not able to treat large kinetic mechanisms; moreover it was implemented for combustion engine. Thus reactingFoam is modified in order to make possible the introduction of detailed chemistry.
The OpenFOAM framework is used to solve the gas-phase transport equations and edcSMOKE is used to manage the interaction between chemistry and turbulence.
Finally, both steady-state solver (*"edcSimpleSMOKE"*) and unsteady-state solver (*"edcPimpleSMOKE"*) are available. Moreover, edcSMOKE is coupled with the OpenSMOKE library developed by Cuoci [12] that is developed to manage large kinetic schemes. The Figure4.1 illustrates, in detail, how the edcSMOKE solver works, the steady state solver is shown but the scheme is the same also for the unsteady. In particular, the interactions between edcSMOKE, the OpenSMOKE library and the OpenFOAM software are reported. The blue box, with continue line, includes more important files of edcSMOKE and their relationships. The kinetic mechanism is interpreted by the solver, through the *"createOpenSMOKEFields.H"*, that transforms the CHEMKIN format (available on Internet) in the XML format, used by OpenSMOKE. At the same time, all the other fields are generated and the code starts to solve all the variables. In particular "UEqn.H" consists of the equations relative to the velocity field, "EEqn.H" in the equations of the enthaply field, finally "YEqn.H" in the mass balance equations. The *edcSMOKE* solver gives the possibility to choose, in the Chemistry.H file, the combustion model between ED (Eddy Dissipation Model) ED-FR (Eddy Dissipation-Finite Rate) and EDC (Eddy Dissipation Concept). In this work the mass balance has been performed through the use of the EDC model, in the blue dashed line box the main files modified are reported. In the "EDC.H" or in the "EDC_DRG.H", the mass balance of the mean flow is performed. The mass fraction of the species in the mean flow ($\overline{\omega}$), the temperature of the cell (T_{cells}), the pressure of the cell (p_{Cells}), the enthalpy of the mean flow ($\overline{h}$), the mass fraction of the fine structure (γ^*), the mass transfer, per unit of mass, between the mean flow and the fine structure ($\dot{m}^*$) and the fraction of the fine structure where the reactions occur

(χ) are evaluated and used to set the PSR in the "ODE_PSR.H". In this file the mass fraction of the species in the fine structures is recovered then updated in the "EDC.H" (or "EDC_DRG.H") file.
Once the velocity field, the enthalpy field and the mass fraction field are established, the problem is solved by coupling the edcSMOKE with the OpenFOAM framework.

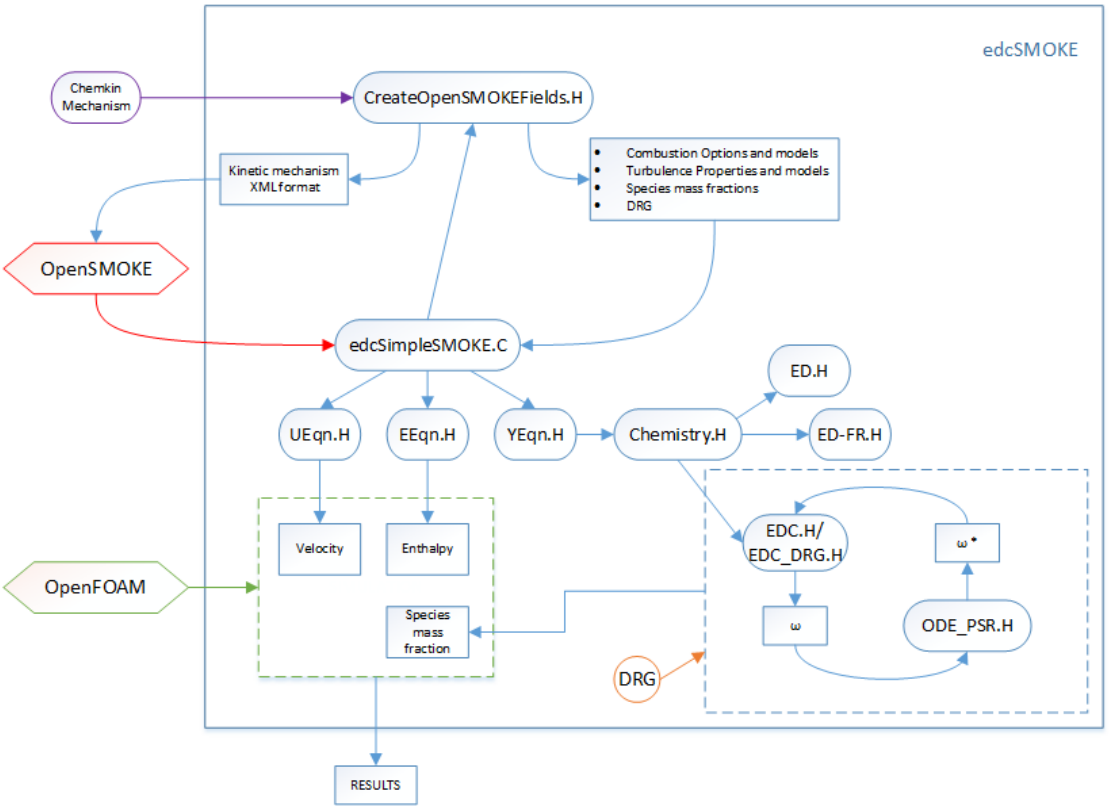

FIGURE 4.1: edcSMOKE framework

4.2 Coupling of DRG with EDC

The DRG code has been coupled with the open source solver *"edcSMOKE"*, used to simulate turbulent flames.
The first step for the coupling was to define a new model in the EDC solver. In order to couple DRG without complicating the EDC code, a new option has been developed. The "EDC_DRG.C" file has been added to *"edcModel"* folder in *"edcSMOKE-master"*. The Figure4.2 illustrate the general framework of edcSMOKE coupled with DRG. In particular it simply shows as OpenSMOKE++, edcSMOKE and OpenFOAM work together in the resolution of a turbulent reactive flow.

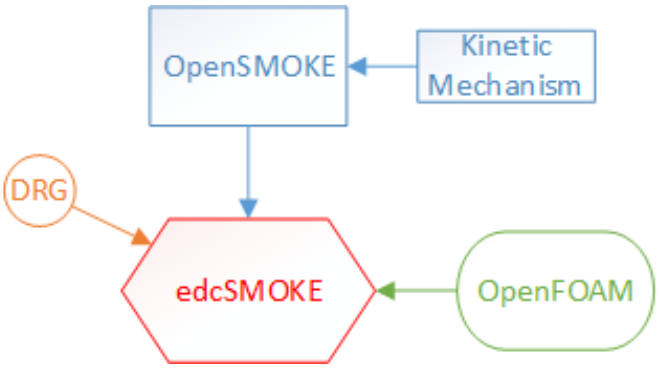

FIGURE 4.2: Coupling of DRG with edcSMOKE

The DRG header code is included in the *"edcSimpleSMOKE.C"* file, in the *"edcSimpleSMOKE"* folder, and in *"edcPimpleSMOKE.C"* file, in the *"edcPimpleSMOKE"* folder, as follows:

```
#include "DRG.h"
```

The possibility to choose the EDC_DRG as solver has been added to the *"chemistry.H"* file in the *edcModel* folder.

4.2.1 EDC_DRG

In the EDC_DRG code, DRG solver is activated if the temperature in the cell is higher than the minimum temperature set in the DRG setting. When this happens, a vector $\overline{\omega}$, with the length equal to the number of species, containing the mass fraction of the species is calculated.
If the DRG is turned on, the solver has to solve a PSR (perfect stirred reactor). In this case, according to the cells temperatures, a ϵ value is taken into account. The relative piece of the code is shown below:

```
if (TCells[celli] > drg_minimum_temperature_for_chemistry)
{
// Extract the mean mass fractions
for(unsigned int i=0;i<NC;i++)
omegaMean[i+1] = Y[i].internalField()[celli];

// Convert to mole fractions
thermodynamicsMapXML->MoleFractions_From_MassFractions(xMean, MWMean, omegaMean);

// Extract the fine strucutres mass fractions
if (reactorType == REACTORTYPE_PSR)
{
```

```
for(unsigned int i=0;i<drg_temperature.size();i++)
if(TCells[celli] < drg_temperature[i])
{
drg->SetEpsilon(drg_epsilon[i]);
break;
}
```

At this point, a vector y_0^*, with the size equal to *(number_important_species + 2)* is used to store the mass fractions of the important species and the temperatures vector. Thus, the star mass fractions ω^* are extracted from the vector of mean flow mass fractions $\overline{\omega}$ and used in the setting of the fine structure.

note: the size of ω^* is equal to the total number of species. This is important because all the species must be considered in the fine structure. During PSR resolution, the DRG code solves the mass balance only with important species and "freeze" the others.

```
double cTot_ = pCells[celli]/PhysicalConstants::R_J_kmol/TCells[celli];
Product(cTot_, xMean, &c_);
drg->Analysis(TCells[celli], pCells[celli], c_);

NEQ = drg->number_important_species()+2;

yStar0.resize(NEQ);
yStarf.resize(NEQ);
yMax.resize(NEQ);       yMax.setConstant(1.); yMax(NEQ-2) = 5000.;      yMax(NEQ-1) = 1.e16;
yMin.resize(NEQ);       yMin.setConstant(0.); yMin(NEQ-2) = 280.;       yMin(NEQ-1) = 0.;

for (unsigned int i=0;i<drg->number_important_species();++i)
{
const unsigned int j = drg->indices_important_species()[i]+1;
yStar0(i) = omegaMean[j];
yStar0(NEQ-2) = TCells[celli];
yStar0(NEQ-1) = 0.;

}

// Extract the star mass fractions
for(unsigned int i=1;i<=NC;i++)
omegaStar[i] = omegaMean[i];

// Set DRG
fine_structure_ode_psr.SetDRG(drg);

// Initialize the fine structure
thermodynamicsMapXML->SetTemperature(TCells[celli]);
thermodynamicsMapXML->SetPressure(pCells[celli]);
thermodynamicsMapXML->hMolar_Mixture_From_MoleFractions(hMean, xMean);
hMean/=MWMean;

fine_structure_ode_psr.Set(TCells[celli], pCells[celli], omegaMean, omegaStar, hMean,
                                            gammaStar[celli], mDotStar[celli], chi);
```

```
tf = numberOfResidenceTimes/max(mDotStar[celli], SMALL);
}
```

The mass fractions field of the important species and the temperature field are generated in order to evaluate both the mean mass transfer R, from the fine structure to the mean flow, and the heat release.

```
for(unsigned int i=0;i<NEQ-2;i++)
{
const unsigned int j = drg->indices_important_species()[i];
YStar_[j].internalField()[celli] = (1.-relaxationFactorFineStructures)*yStar0(i) +
 relaxationFactorFineStructures*yStarf(i);
}
TStar_[0].internalField()[celli] = (1.-relaxationFactorFineStructures)*yStar0(NEQ-2) +
 relaxationFactorFineStructures*yStarf(NEQ-2);

for(unsigned int i=0;i<NEQ-2;i++)
R_[i].internalField()[celli] = edc_coefficient[celli]*(YStar_[i].internalField()[celli]-
                                                       - Y[i].internalField()[celli]);

thermodynamicsMapXML->SetTemperature(TCells[celli]);
thermodynamicsMapXML->SetPressure(pCells[celli]);
thermodynamicsMapXML->hMolar_Species(h_species);

double HeatRelease = 0.;
for(unsigned int i=0;i<NC;i++)
```

Finally, the "*important_reactions*" and the "*important_species*" fields, defined in *"createFields.H"* in the *"edcSimpleSMOKE"* folder, are updated.

```
}
getchar();
}

// Fill the relevant DRG fields
drgSpeciesCells[celli]   = drg->number_important_species();
drgReactionsCells[celli] = drg->number_important_reactions();
}
else
{
```

4.2.2 ODE_PSR

In the header file *"ODE_PSR.H"* the public member **SetDRG** is defined:

```
void SetDRG(OpenSMOKE::DRG* drg) {drg_=drg; drgAnalysis_=true;}
```

In the *"ODE_PSR.C"* the mass balance relative to the fine structure is solved.
The mass fractions of the important species are recovered and stored in ω^*. Since the volume of interest includes also the surrounding fluid, a mass fraction of the surrounding fluid, ω_{Surr} is calculated.

```
}
else if (drgAnalysis_ == true)
{
//Recover mass fractions
if (checkMassFractions_ == true)
{
for (unsigned int i=0;i<drg_->number_important_species();++i)
{
const unsigned int j = drg_->indices_important_species()[i]+1;
omegaStar_[j] = max(y[i+1], 0.);
}
}
else
{
for (unsigned int i=0;i<drg_->number_important_species();++i)
{
const unsigned int j = drg_->indices_important_species()[i]+1;
omegaStar_[j] = y[i+1];
}
}

// Recover temperature
unsigned int index_TStar = drg_->number_important_species()+1;
TStar_ = y[index_TStar];

// Recover dummy variable
const double dummy_ = y[drg_->number_important_species()+2];

for(unsigned int i=0;i<drg_->number_important_species();++i)
{
const unsigned int j = drg_->indices_important_species()[i]+1;
omegaSurr_[j] = (omegaMean_[j] - omegaStar_[j]*gammaStar_*chi_)/(1.-gammaStar_*chi_);
```

Finally, the useless reactions are removed from the r_{Star} vector, where the reaction rates are stored and the formation rate of the species is evaluated through the value of r_{Star} obtained.

```
// Remove useless reactions
for (unsigned int i=0;i<drg_->indices_unimportant_reactions().size();++i)
rStar_[drg_->indices_unimportant_reactions()[i]+1] = 0.;

// Formation rates
```

```
kineticsMapXML_.stoichiometry().FormationRatesFromReactionRates(&RStar_, rStar_);

// Recovering residuals
for (unsigned int i=0;i<drg_->number_important_species();++i)
{
const unsigned int j = drg_->indices_important_species()[i]+1;
dy[i+1] = thermodynamicsMapXML_.MW()[j]*RStar_[j]/rhoStar_ + mDotStar_*(omegaSurr_[j]-
                                                                        -omegaStar_[j]);
}
```

Chapter 5

DRG simulation of turbulent flames

In order to obtain a validation of DRG method implemented in EDC model, different simulations have been performed. A Sandia flame D [23] has been simulated, initially using the EDC model with the complete kinetic mechanism and, in a second time, turning on the DRG method. A set of different conditions for DRG have been used in order to evaluate the sensitivity of this method to the initial parameters, i.e. species, epsilon and temperature have been changed. Finally the results of complete kinetic mechanism are compared with those obtained using DRG.

5.1 Numerical Model and solution techniques

The flame simulated was widely studied by R. S. Barlow and J. H. Frank and described in [24], [23]. The main inner jet has a diameter d_{jet} = 7.2mm, the pilot annulus outer diameter d_{pilot}= 18.2mm and a thickness of the wall between the main jet and the pilot jet of 0.25mm, finally the burner outer wall diameter is of d_{outer}=18.9mm. The main jet velocity, at 294K and 1atm, is assumed to be $\nu_{fuel} = 49.6m/s$. The coflow is composed of air with a velocity of $\nu_{air} = 0.9m/s$. Finally, the pilot bulk velocity is equal to $\nu_{pilot} = 11.4m/s$. The molar compositions of the three different flow are reported in the Table5.1:

5.1.1 Numerical grid

A structured mesh of 4608 cells has been used for the simulations. Specifically, the mesh is uniformly spaced with Δx = 1cm for $0 \leq x \leq$ 11cm with increasingly larger spacing

	MAIN JET	**COFLOW JET**	**PILOT JET**
CH_4	0.1561	-	-
O_2	0.1966	0.23	0.0540
N_2	0.6473	0.77	0.7342
H_2O	-	-	0.0942
CO_2	-	-	0.1098
OH	-	-	0.0028

TABLE 5.1: Mole fractions of different flows in Sandia burner

from here to the end of the chamber, and it is also uniformly spaced with $\Delta y = 0.18$cm for $0 \leq x \leq 1.8$cm with increasingly larger spacing for $1.8 \leq x \leq 14$cm. The schematic for the mesh is reported in Figure5.1.

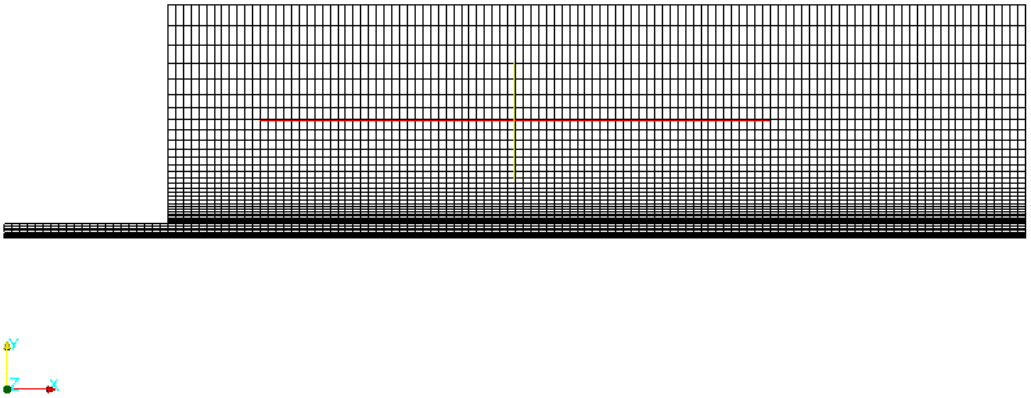

FIGURE 5.1: Computational Grid

5.1.2 Physical Models

The chemical mechanism employed is GRI-Mech version 3.0, consisting of 53 chemical species and 325 reversible reactions.
The DRG has to be set in the *"solverOption"* file, contained in the *"costant"* folder.
The setting required a minimum temperature value (minTemperature), a vector of temperatures (of size 2 in this case) and a threshold value, ϵ, that is function of temperature, so it is possible to set two different values of ϵ, one is used below the lowest temperature and another value, smaller than the first one, that is used in the reaction zone.
Three different cases have been simulated in order to evaluate the sensitivity of the model to the parameters of DRG. The Table5.2, Table5.3 and Table5.4 show the parameters set for the three different cases. In particular Table5.2 and Table5.3 have the same threshold values and the same temperature range and they differ for the species,

while between Table5.3 and Table5.4 the difference is relative to the threshold values.

DRG-case1	
minT	280
temperature	700 4000
epsilon	1e-1 1e-2
species	CH_4 O_2 OH

TABLE 5.2: DRG-case1

DRG-case2	
minT	280
temperature	700 4000
epsilon	1e-1 1e-2
species	CH_4 HO_2 CO

TABLE 5.3: DRG-case2

DRG-case3	
minT	280
temperature	700 4000
epsilon	1e-2 1e-2
species	CH_4 HO_2 CO

TABLE 5.4: DRG-case3

5.1.3 Results

In the following section the results obtained from the simulations are shown. In particular the trends of the temperature and of the mole fractions of the major species along the flame centerline are reported. In order to validate the DRG method, the computational results obtained with the complete kinetic mechanism have been compared with those obtained using DRG method.
A sensitivity analysis of the DRG method at the initial parameters has been performed, therefore, in the following, are shown:

- Comparison between values of the simulations with complete kinetic mechanism and applying DRG method with different initial set of species. In particular the first set consists of CH_4, O_2 and OH and the second one consists of CH_4, HO_2 and CO.

- Comparison between values of the simulations with complete kinetic mechanism and applying DRG method with different threshold values. In particular the common set of species consists of CH_4, HO_2 and CO. The case 1 works with a ϵ value

of 1e-1 below 700K and of 1e-2 between 700K and 4000K (this value is very high but has been chosen to be sure that the maximum temperature of the flame was smaller than this one), while the case 2 works with the same value of ϵ, equal to 1e-2, for every temperature.

Different initial set of species

The **temperatures** profiles along the centerline are shown in Figure5.2. In all the cases, complete kinetic, first set of key species and second set of species, the trades are quite the same. Indeed, the maximum value of the temperature, T_{max}, is equal to 2130K and located at 61cm from the gas inlet, with complete kinetic,it is 2134K, at 59.6cm from the gas inlet, with CH_4, O_2 and OH as set of initial species, and is 2127K located at 59cm from the gas inlet for the second set of species (CH_4, HO_2, CO). The errors relative to the maximum temperature are around 0.2% in the first case and around 0.1% in the second one. A small difference is present in the range between 20cm and 30cm from the inlet gas where the temperature, evaluated through DRG, grows faster than the other. As subsequently shown, this behaviour partly results to the lower temperature, imposed in DRG setting, that is very close to this area and to the threshold values imposed. A similar behaviour is shown by CO_2.

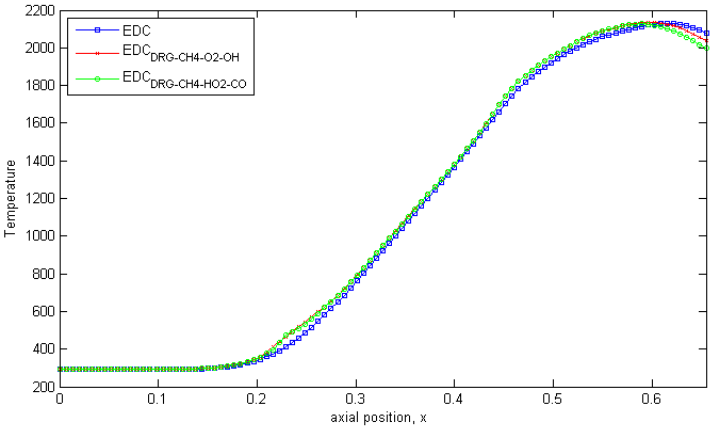

FIGURE 5.2: Axial profiles of temperature (T), in K, along the flame centerline as functions of nondimensional axial position (z/H_T). The results of two cases of DRG analysis, with two different species set, are compared with the numerical simulation without the reduction of kinetic mechanism

The Figure5.3 shows the shapes of **CH_4 mole fraction** along the centerline. EDC and both cases of EDC_{DRG}, show the same behaviour in the first part of the burner, where the temperature is below 700K, in the reactive zone, where the DRG takes into account a lot of the reactions, and far from the inlet zone where X_{CH_4} is very low. As with the

temperature shape, EDC_{DRG} shows some discrepancies in $20 \leq x \leq 30$cm and in the "post-combustion" area. However the results are in full agreement with the expectation because CH_4 is one of the species of the key set of DRG, in both cases.

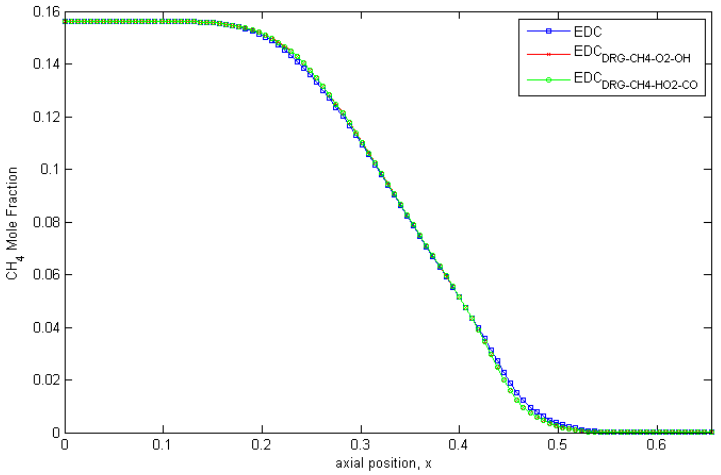

FIGURE 5.3: Axial profiles of CH_4 mole fraction (X_{CH_4}) along the flame centerline as functions of nondimensional axial position (z/H_T). The results of two cases of DRG analysis, with two different species set, are compared with the numerical simulation without the reduction of kinetic mechanism

Mole fractions of O_2 along the centerline are illustrated in Figure5.4. The behaviour, of all the cases, is similar to the one seen for the CH_4. Indeed the curves(about O_2) are completely overlapping, except that for the same two areas of the methane. It is also present a more marked difference in the area downstream of the flame where the maximum error reaches is around 47% in the first case and 59% in the second one. However, these values are relative to low mole fractions. Since the mole fraction in this area is overestimated, it is possible that DRG is not considering all the reactions that are O_2 consuming, but it is also true that in the first case the O_2 is present in the key set of species.

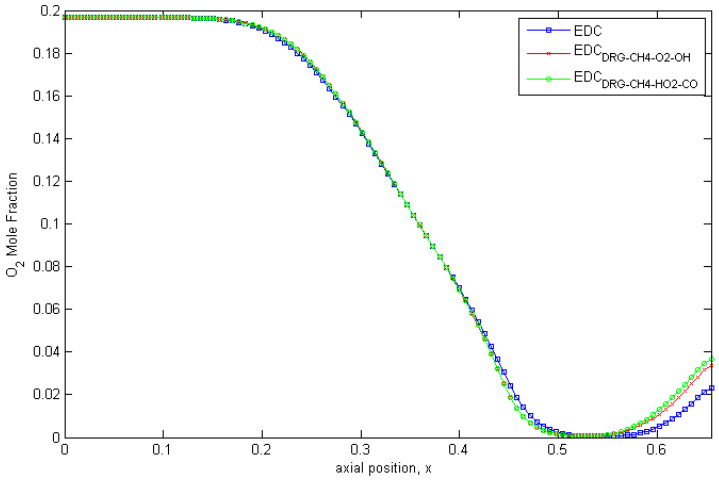

FIGURE 5.4: Axial profiles of O_2 mole fraction (X_{O_2}) along the flame centerline as functions of nondimensional axial position (z/H_T). The results of two cases of DRG analysis, with two different species set, are compared with the numerical simulation without the reduction of kinetic mechanism

Mole fractions of H_2O along the centerline are illustrated in Figure5.5. Also in this case, DRG behaviour agrees with EDC results. As a matter of fact, the three curves overlap completely, for the whole length of the burner, except that for the last part, the same interesting O_2. The maximum error, between EDC and EDC_{DRG}, is around 7% and is relative to the second case.

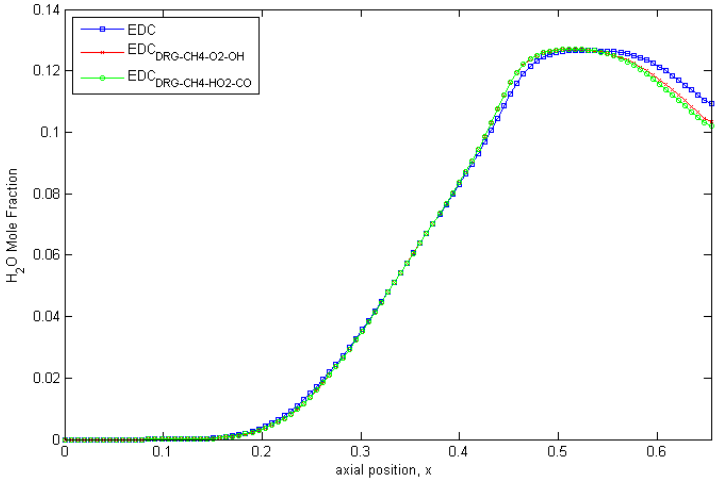

FIGURE 5.5: Axial profiles of H_2O mole fraction (X_{H_2O}) along the flame centerline as functions of nondimensional axial position (z/H_T). The results of two cases of DRG analysis, with two different species set, are compared with the numerical simulation without the reduction of kinetic mechanism

The results about **CO_2 mole fractions**, see Figure5.6, show a significant difference between the values using the complete kinetic mechanism and those using DRG. In particular the trend between 20cm and 30cm, from the gas inlet, is probably due to the wrong evaluation of temperature(and vice versa). As subsequently shown, the difference between the case with and without DRG, is caused by the number of species, thus by the number of reactions, taken into account. In particular this area is close to 700K, thus it is close to the border at which DRG changes threshold value. Therefore the impact of DRG depends on epsilon values and on the relative temperature. The maximum value of the error is equal to 11%.

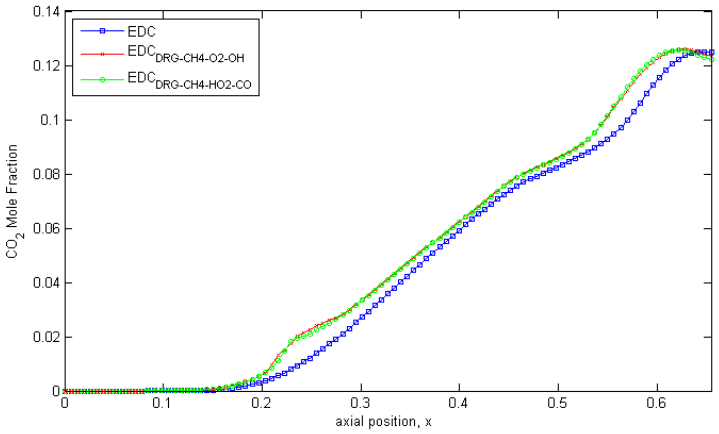

FIGURE 5.6: Axial profiles of CO_2 mole fraction (X_{CO_2}) along the flame centerline as functions of nondimensional axial position (z/H_T). The results of two cases of DRG analysis, with two different species set, are compared with the numerical simulation without the reduction of kinetic mechanism

OH mole fractions are reported in Figure5.7. The two curves, relative to DRG simulations, are shifted to the entrance of the chamber. In particular the peak of the first case is shifted, with respect to the values relative to the complete kinetic mechanism, of 2cm in the direction of the gas inlet an is overestimated by about 4%, while in the second case the curve is shifted of 2.5cm and the peak is overestimated by about 3%.

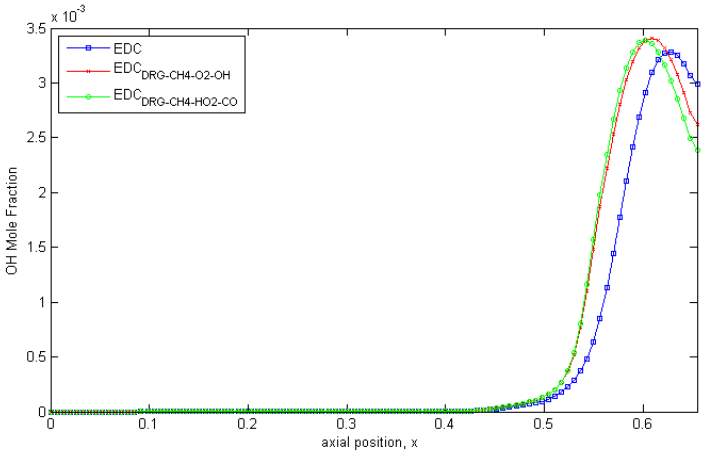

FIGURE 5.7: Axial profiles of OH mole fraction (X_{OH}) along the flame centerline as functions of nondimensional axial position (z/H_T). The results of two cases of DRG analysis, with two different species set, are compared with the numerical simulation without the reduction of kinetic mechanism

Finally the **trend of the number of important species and the trend of the number of important reactions** are showed in Figure5.8 and in Figure5.9. As expected, the area where the DRG takes into account a bigger number of species and reactions is the hottest one, where the combustion takes place. As expected, the trends of the number of species, thus the number of reactions, follow the concentration profiles of the species of the initial set. As a matter of fact the number of species of case1 is high where the OH concentration is high, while the second case shows a significant activity where the concentration of HO_2 is higher.

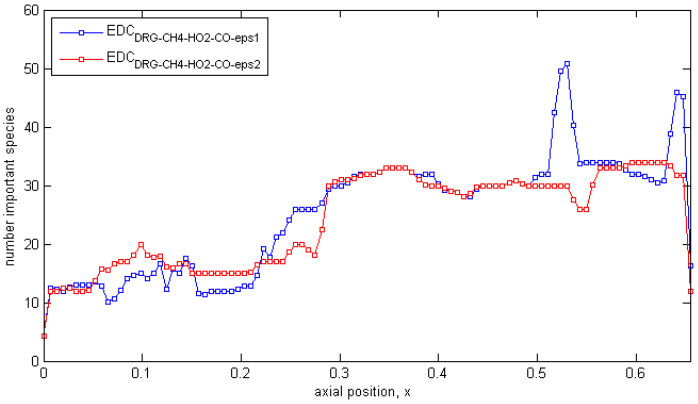

(A)

FIGURE 5.8: Axial trend of number of important species along the flame centerline as functions of nondimensional axial position (z/H_T). The results of the two cases of DRG analysis, with two different species set, are compared

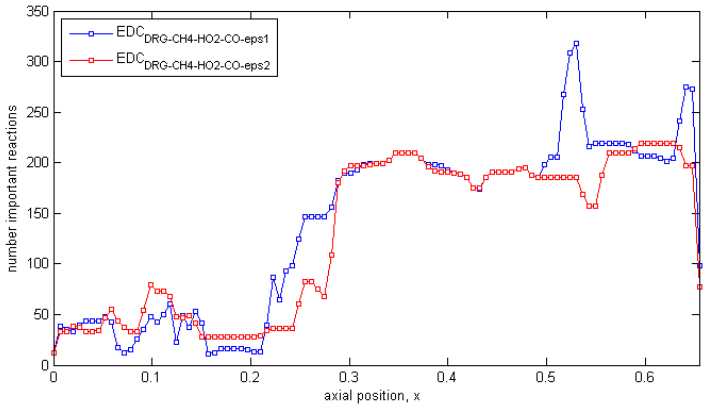

(A)

FIGURE 5.9: Axial trend of number of important species along the flame centerline as functions of nondimensional axial position (z/H_T). The results of the two cases of DRG analysis, with two different species set, are compared

Different threshold value (ϵ)

The **temperature** profiles along the centerline are shown in Figure5.10. In all the cases, complete kinetic and both set of threshold values, the trades are quite the same. Indeed, the maximum value of the temperature, T_{max}, is equal to 2130K and located at 61cm from the gas inlet, with complete kinetic, it is 2127K located at 59cm from the gas inlet for the first set of threshold values (1e-1 1e-2), finally the peak of temperature is 2124K, at 59cm from the inlet, for the second set of ϵ (1e-2 1e-2). In both cases, the error relative to the maximum temperature is around 0.1%. As expected, using a lower threshold value gives more accurate results because the DRG method takes into account

more species and reactions. The second set of ϵ, as a matter of fact, shows a trend that is more similar to the complete kinetic results than to the first case of DRG. The strange behaviour in the range between 20cm and 30cm, from the gas inlet, shown by the first set of threshold values is not present in the second case demonstrating that this problem derives from DRG set of temperature. As a matter of fact, choosing a lower value of temperature, relative to the lower value of ϵ, DRG should be capable to properly evaluate the temperature trend in this area. The same is also true for the concentration of the species.

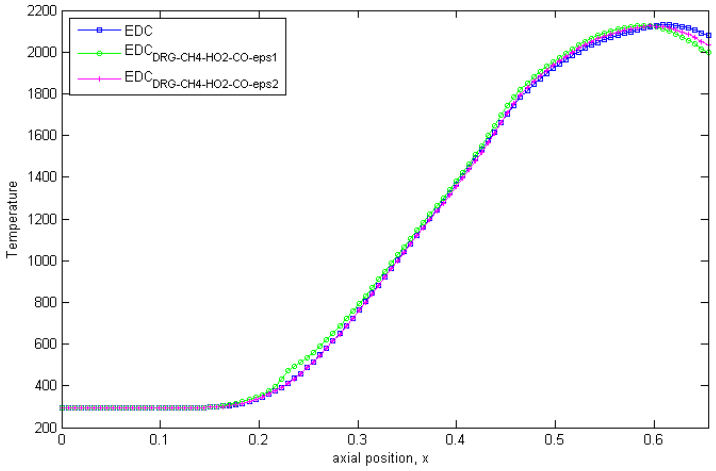

FIGURE 5.10: Axial profiles of temperature (T), in K, along the flame centerline as functions of nondimensional axial position (z/H_T). The results of two cases of DRG analysis, with two different set of ϵ, are compared with the numerical simulation without the reduction of kinetic mechanism

The Figure5.11 shows the shapes of **CH_4 mole fraction** along the centerline. EDC and both the cases of EDC_{DRG}, show the same behaviour along all the length of the burner. As for the temperature, the results from the second set of threshold values are more accurate than the first set but in both cases the accuracy is very high. These results are in full agreement with the expectation because CH_4 is one of the species of the key set of DRG, in both cases.

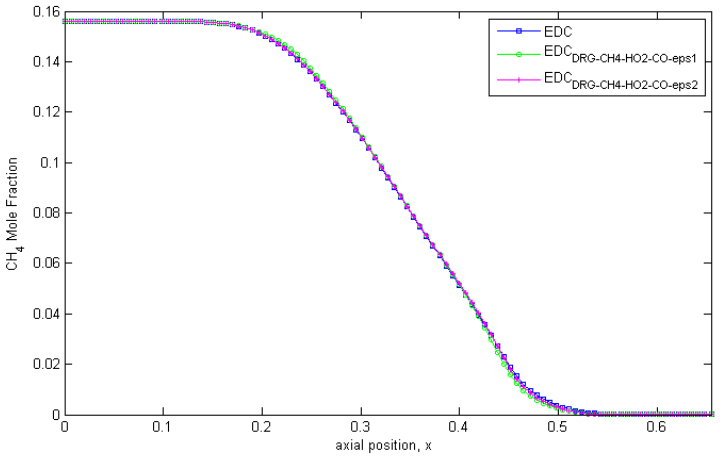

FIGURE 5.11: Axial profiles of CH_4 mole fraction (X_{CH_4}) along the flame centerline as functions of nondimensional axial position (z/H_T). The results of two cases of DRG analysis, with two different set of ϵ, are compared with the numerical simulation without the reduction of kinetic mechanism

Mole fractions of O_2 along the centerline are illustrated in Figure5.12. The behaviour, of all the cases, is similar to the one seen for the CH_4. Indeed the curves(about O_2) are completely overlapping, except that for the end of the burner where the maximum error reached is around 59% in the first case and 40% in the second one. However, these values are relative to low mole fractions. Since the mole fraction in this area is overestimated, it is possible that DRG is not considering all the reactions that are O_2 consuming and it is also possible to have more accuracy in this area, adding another species, typically present in the exhaust gas, in the key set of species.

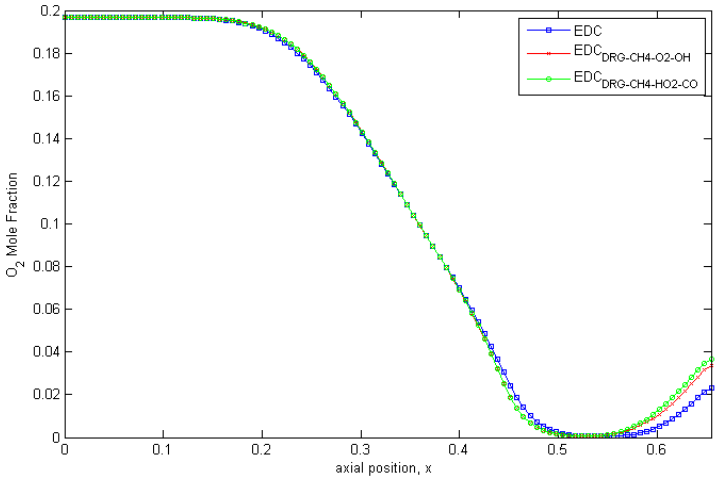

FIGURE 5.12: Axial profiles of O_2 mole fraction (X_{O_2}) along the flame centerline as functions of nondimensional axial position (z/H_T). The results of two cases of DRG analysis, with two different set of ϵ, are compared with the numerical simulation without the reduction of kinetic mechanism

Mole fractions of H_2O along the centerline are illustrated in Figure5.13. Also in this case, DRG behaviour agrees with EDC results. As a matter of fact, the three curves overlap completely, for the whole length of the burner, except that for the last part, the same interesting O_2. The maximum error, between EDC and EDC_{DRG}, is around 7% and is relative to the second case. As said for O_2, more accurate trends could be obtained using a set of species that include product species.

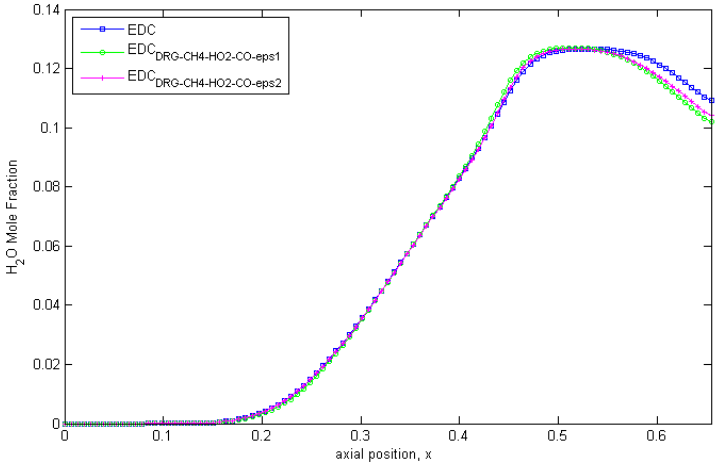

FIGURE 5.13: Axial profiles of H_2O mole fraction (X_{H_2O}) along the flame centerline as functions of nondimensional axial position (z/H_T). The results of two cases of DRG analysis, with two different set of ϵ, are compared with the numerical simulation without the reduction of kinetic mechanism

The results about **CO_2 mole fractions**, see Figure5.14, show some difference between the values using the complete kinetic mechanism and those using DRG. In particular, as shown in the previous section, the first set of epsilon is not very accurate, especially between 20cm and 30cm from the gas inlet, while the second set is in good agreement in the first part of the burner, less close to the outlet, as for the mole fractions of the other species. These results demonstrate that, the first case is not able to properly describe the first part between 20cm and 30cm because of the ϵ and/or the temperature. Using a lower value of epsilon, or a lower value of the temperature, the accuracy increases but, on the other way, the higher is the accuracy, higher is the computational time.
The maximum value of the error is equal to 11%, relative to the first case.

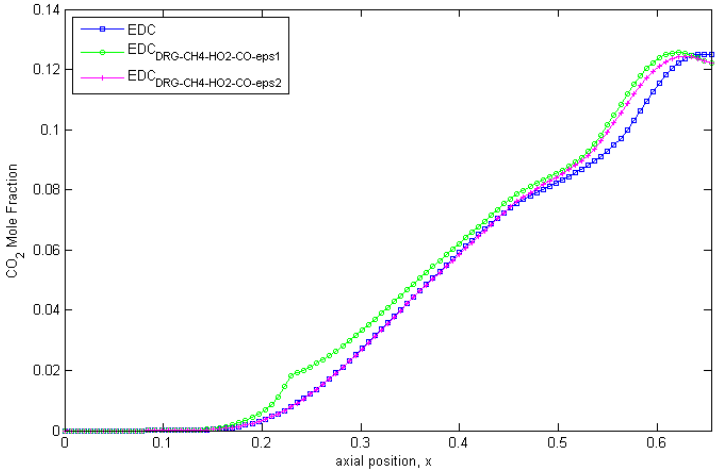

FIGURE 5.14: Axial profiles of CO_2 mole fraction (X_{CO_2}) along the flame centerline as functions of nondimensional axial position (z/H_T). The results of two cases of DRG analysis, with two different set of ϵ, are compared with the numerical simulation without the reduction of kinetic mechanism

OH mole fractions are reported in Figure5.15. The two curves, relative to DRG simulations, are shifted to the entrance of the chamber. In particular the peak of the first case is shifted, with respect to the values relative to the complete kinetic mechanism, of 2.5cm in the direction of the gas inlet and it is overestimated by about 3%, while in the second case the curve is shifted of 2cm and the peak is overestimated by about 2%.

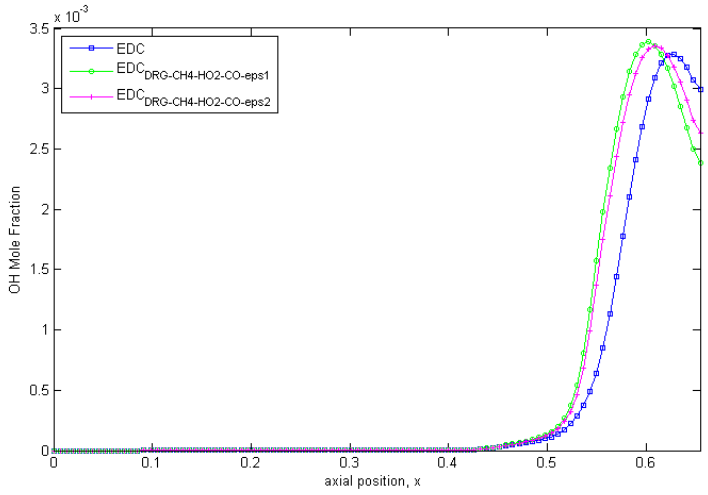

FIGURE 5.15: Axial profiles of OH mole fraction (X_{OH}) along the flame centerline as functions of nondimensional axial position (z/H_T). The results of two cases of DRG analysis, with two different set of ϵ, are compared with the numerical simulation without the reduction of kinetic mechanism

Finally the **trend of the number of important species and the trend of the number of important reactions** are showed in Figure5.16 and in Figure5.17. As expected, the trend of the second set of ϵ shows a bigger number of species, then reactions, taken into account with to respect the first set along almost the entire length of the burner, especially in the first part. The same behaviour, instead, is shown in the combustion area where the number of species and reactions taken into account in both cases is the same. Finally, these results show as ϵ equal to 1e-2, for all the temperatures, is a value too much low because the reduction of the kinetic mechanism is not very efficient.

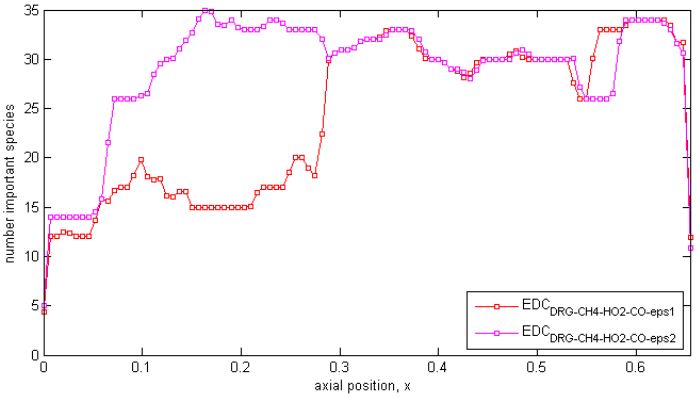

(A)

FIGURE 5.16: Axial trend of number of important species along the flame centerline as functions of nondimensional axial position (z/H_T). The results of the two cases of DRG analysis, with two different set of ϵ, are compared

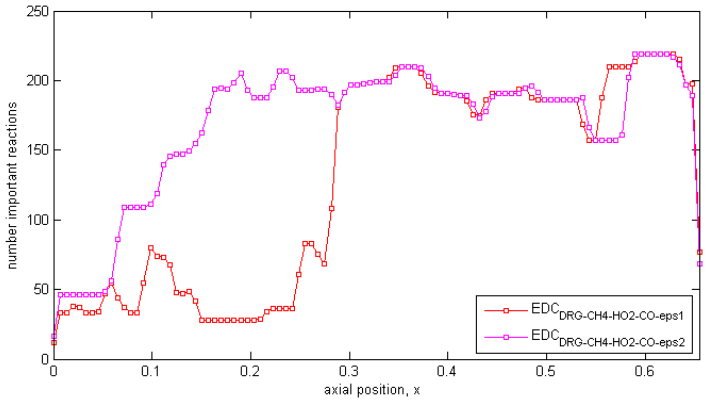

(A)

FIGURE 5.17: Axial trend of number of important species along the flame centerline as functions of nondimensional axial position (z/H_T). The results of the two cases of DRG analysis, with two different set of ϵ, are compared

5.1.4 Conclusion

The simulations have been run in parallel with the same number of processors. Table5.5 shows the time to convergence of the different cases. In particular, it is possible to compare the complete kinetic mechanism case and the three different cases of DRG.

Case	Time [hr]
Complete Kinetic	≈ 112
DRG-case1	≈ 75
DRG-case2	≈ 70

TABLE 5.5: Comparison of time to convergence between the complete kinetic mechanism case and the different cases of DRG method

As expected, the DRG method reduced the CPU time and predicts almost the same results of the case with the complete detailed mechanism.
Obviously, incrementing the accuracy of the results requires an increment of the computational time. As a matter of fact, as expected, the case3 presents a time saving that is lower than the other DRG cases, but the values obtained are closer to those from the simulation with complete chemistry. Therefore, a good compromise between accuracy and computational time could be obtained, in this case, using an ϵ value, for the range of temperature below 700K, higher than the DRG-case2 but higher than DRG-case3 in order to reduce the number of species and reactions in the first part of the burner.
As shown, the set key species have a certain influence on the results, especially in the end of the burner, but it is less important than the ϵ value. Indeed the computational time, between DRG-case2 and DRG-case3, is almost the same.
Finally, in B the contour plot of the different cases are reported. In particular, those relative to the number of important species and number of important reactions show clearly the influence of the set of DRG. Indeed DRG-case1 and DRG-case2 are very similar in both range and distribution in the chamber, while DRG-case3 shows an intense activity in the border between the combustion zone and the fresh air where almost all the species, therefore reactions, are taken into account.

Chapter 6

Conclusions

The present Master thesis wanted to implement the DRG method in an open source code for turbulent combustion modelling. To do that, firstly the DRG method, as implemented in a previous thesis work, has been validated in laminar conditions. Specifically, formation of soot precursors in laminar flame has been studied using a kinetic mechanism consisting of 300 chemical species and 11790 reversible reactions while, for the turbulent flame, the edcSMOKE solver has been firstly modified in order to be capable to use DRG method, and secondly a Sandia D flame has been simulated using a GRI3.0 kinetic mechanism.

As far the laminar case is concerned, the DRG results are in good agreement with the case using complete kinetic mechanism and in particular the results relative to the BIN species (where BIN is name gives to the soot precursors in the kinetic mechanism in use). The advantage in CPU time consuming is around of the 45%. A previous work indicates the time saving in approximately 40%, this means that the time saving increases with the complexity of the system, in this case with the number of reactants.

Subsequently, the DRG has been coupled with the EDC combustion model to allow its use in RANS-based turbulent combustion modelling. The coupling has been done adding a new file to the solver, edcSMOKE, and modifiyng some other files already present in order that the solver was capable to update the mass fraction of the species considering only the important species evaluated through the DRG code. The implementation has been validated through simulations of Sandia D flame that has been chosen because of the number of informations about the burner, about the initial conditions and because the edcSMOKE was validated using this kind of flame, in a previous work. Results were encouraging showing a large agreement between simulations performed with detailed or DRG-reduced schemes. Moreover the results confirmed that the on-the-fly using of DRG method, in these specific simulations, gets advantages in CPU time consuming, by of approximately 30% - 35%.

Further improvements of the work will be aimed at applying the DRG method to more complex simulation, in both geometrical and chemical aspects, in order to evaluate if the computational time saved increases as for the laminar simulation without loosing in accuracy.
Finally the implementation of more complex and accurate on-the-fly methods (e.g. DRG-EP) could be taken into account as new step in dynamic chemical reductions.

Appendix A

Laminar flame contour plots

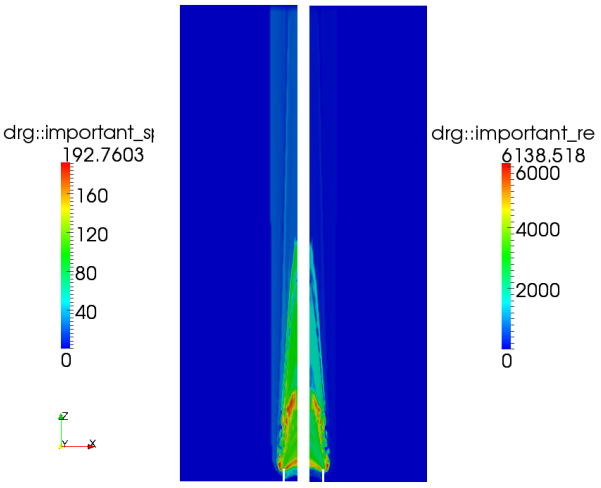

FIGURE A.1: Contour plot of important species and important reactions.

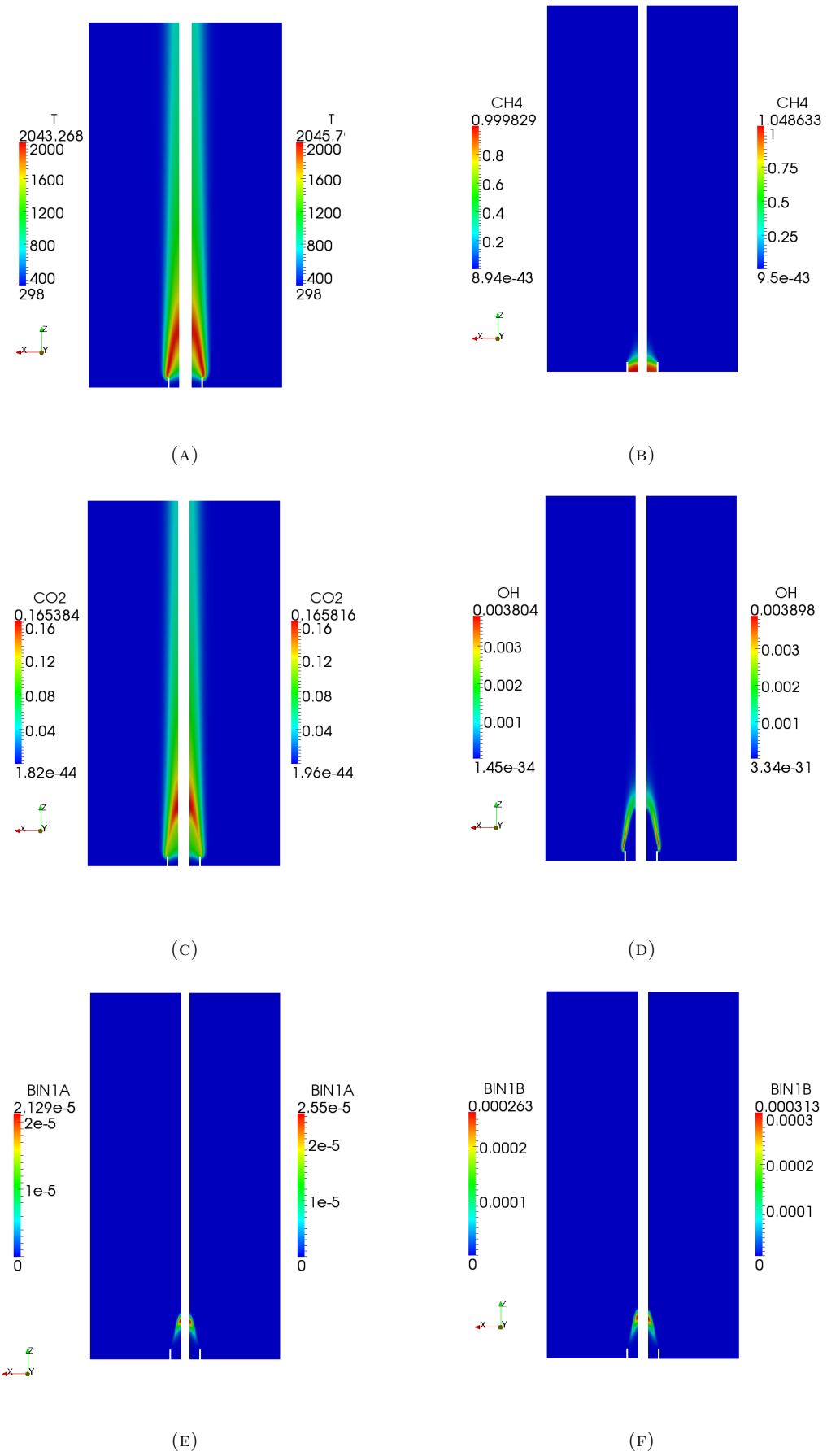

FIGURE A.2: Contour plot of mass fractions (X) of major species and soot precursors, and of temperature (T, in K). The DRG results (left side) and the complete kinetic mechanism (right side) are compared. (A) Temperature, (B) CH_4 mass fraction X_{CH_4}, (C) CO_2 mass fraction X_{CO_2}, (D) OH mass fraction X_{OH}, (E) BIN1A mass fraction X_{BIN1A}, (F) $BIN1B$ mass fraction X_{BIN1B}

Appendix B

Turbulent flame contour plots

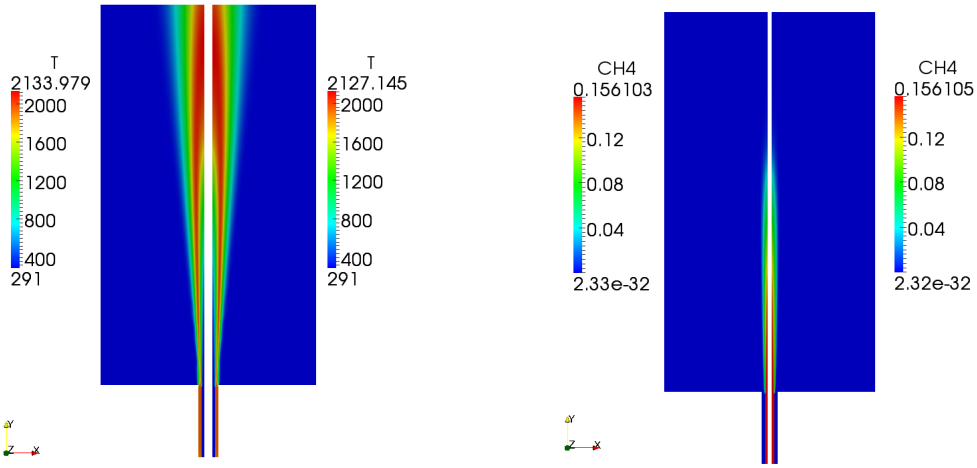

(A)

(B)

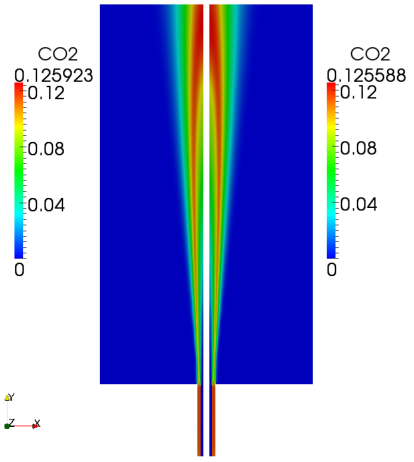

(C)

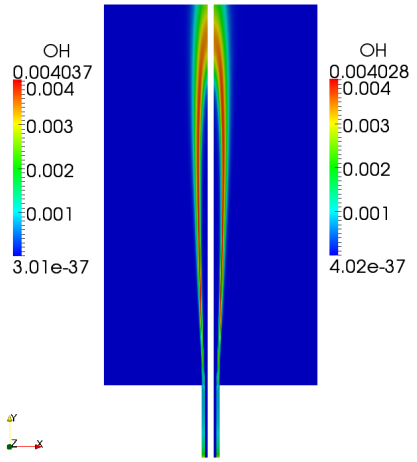

(D)

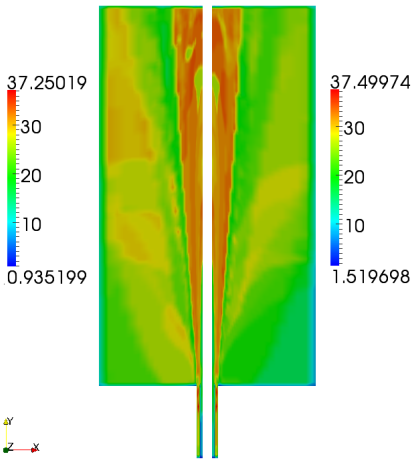

(E)

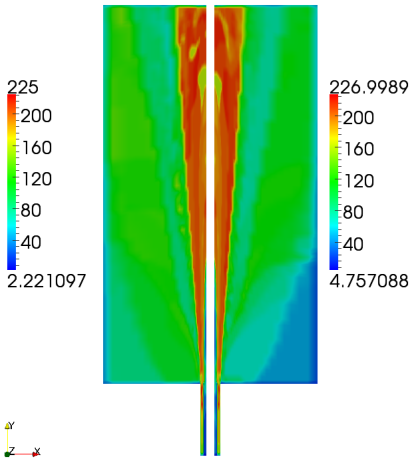

(F)

FIGURE B.1: Contour plot of mass fractions (X) of major species, of temperature (T, in K) and of number of important species and reactions. The DRG-case1 (left side) and DRG-case2 (right side) are compared. (A) Temperature, (B) CH_4 mass fraction X_{CH_4}, (C) CO_2 mass fraction X_{CO_2}, (D) OH mass fraction X_{OH}, (E) Number of important species, (F) Number of important reactions

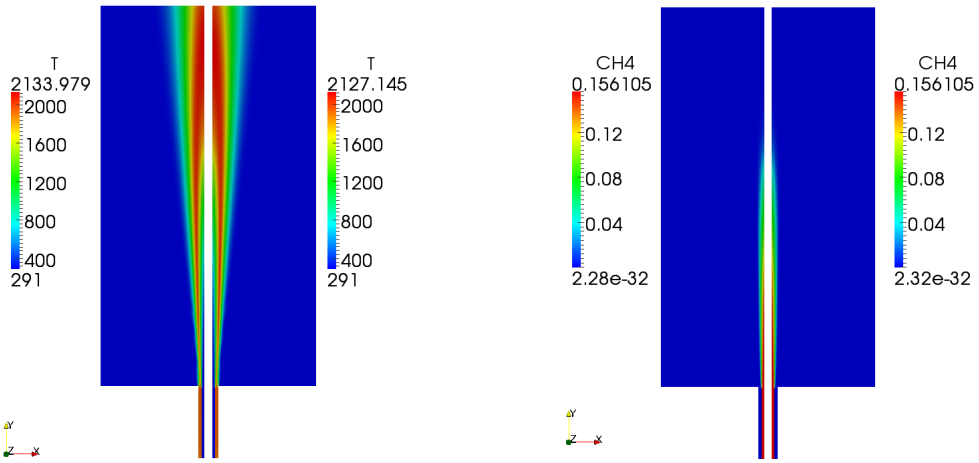

(A)

(B)

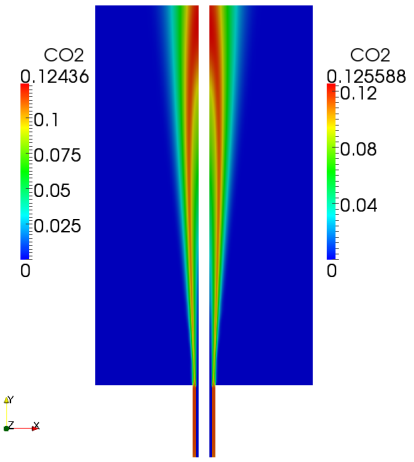

(C)

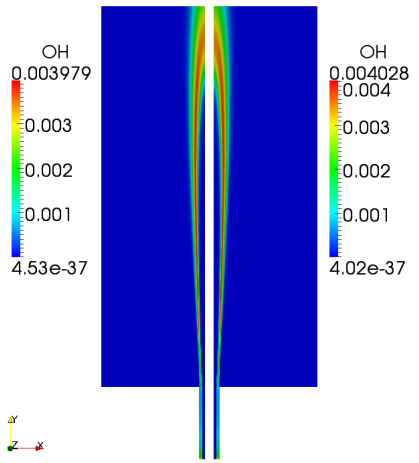

(D)

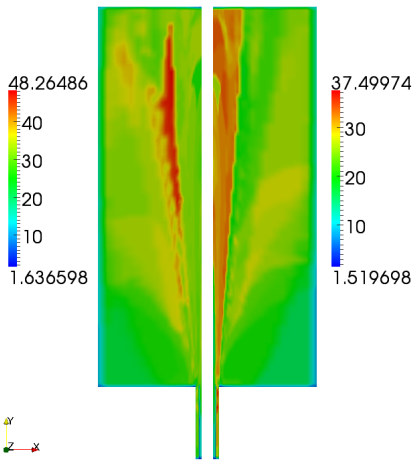

(E)

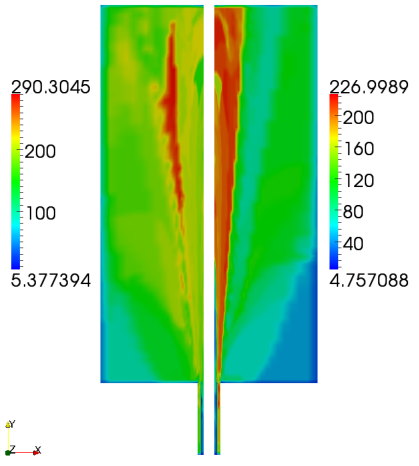

(F)

FIGURE B.2: Contour plot of mass fractions (X) of major species, of temperature (T, in K) and of number of important species and reactions. The DRG-case1 (left side) and DRG-case2 (right side) are compared. (A) Temperature, (B) CH_4 mass fraction X_{CH_4}, (C) CO_2 mass fraction X_{CO_2}, (D) OH mass fraction X_{OH}, (E) Number of important species, (F) Number of important reactions

Bibliography

[1] Beth Anne V Bennett, Charles S McEnally, Lisa D Pfefferle, and Mitchell D Smooke. Computational and experimental study of axisymmetric coflow partially premixed methane/air flames. *Combustion and Flame*, 123(4):522–546, 2000. ISSN 00102180. doi: 10.1016/S0010-2180(00)00158-9.

[2] Valentina Fortunato, Chiara Galletti, Leonardo Tognotti, and Alessandro Parente. Influence of modelling and scenario uncertainties on the numerical simulation of a semi-industrial flameless furnace. *Applied Thermal Engineering*, 76:324–334, 2015. ISSN 13594311. doi: 10.1016/j.applthermaleng.2014.11.005.

[3] Tianfeng Lu and Chung K. Law. A directed relation graph method for mechanism reduction. *Proceedings of the Combustion Institute*, 30(1):1333–1341, 2005. ISSN 15407489. doi: 10.1016/j.proci.2004.08.145.

[4] P. Pepiot-Desjardins and H. Pitsch. An automatic chemical lumping method for the reduction of large chemical kinetic mechanisms. *Combustion Theory and Modelling*, 12:1089–1108, 2008. ISSN 1364-7830. doi: 10.1080/13647830802245177.

[5] J C Keck and D Gillespie. Rate-controlled partial-equilibrium method for treating reacting gas mixtures. *Combustion and Flame*, 17(2):237–241, 1971. ISSN 00102180. doi: 10.1016/S0010-2180(71)80166-9.

[6] S.B. Pope. Computationally efficient implementation of combustion chemistry using in situ adaptive tabulation. *Combustion Theory and Modelling*, 1:41–63, 1997. ISSN 1364-7830. doi: 10.1088/1364-7830/1/1/006.

[7] James C. Sutherland and Alessandro Parente. Combustion modeling using principal component analysis. *Proceedings of the Combustion Institute*, 32(1):1563–1570, 2009. ISSN 15407489. doi: 10.1016/j.proci.2008.06.147.

[8] Francesco Contino, Hervé Jeanmart, Tommaso Lucchini, and Gianluca D'Errico. Coupling of in situ adaptive tabulation and dynamic adaptive chemistry: An effective method for solving combustion in engine simulations. *Proceedings of the*

Combustion Institute, 33(2):3057–3064, 2011. ISSN 15407489. doi: 10.1016/j.proci.2010.08.002.

[9] John P Longwell. The formation of polycyclic aromatic hydrocarbons by combustion. pages 1339–1350, 1982.

[10] R. J. Santoro and H. G. Semerjian. Soot formation in diffusion flames: Flow rate, fuel species and temperature effects. *Symposium (International) on Combustion*, 20:997–1006, 1985. ISSN 00820784. doi: 10.1016/S0082-0784(85)80589-0.

[11] Alberto Cuoci, Alessio Frassoldati, Tiziano Faravelli, and Eliseo Ranzi. A computational tool for the detailed kinetic modeling of laminar flames: Application to C2H4/CH4 coflow flames. *Combustion and Flame*, 160(5):870–886, 2013. ISSN 00102180. doi: 10.1016/j.combustflame.2013.01.011.

[12] A Cuoci, A Frassoldati, T Faravelli, and E Ranzi. OpenSMOKE++: An object-oriented framework for the numerical modeling of reactive systems with detailed kinetic mechanisms. *Computer Physics Communications*, 2015. ISSN 0010-4655. doi: 10.1016/j.cpc.2015.02.014.

[13] PoliMi. POLIMI_PFR_PAH_LT_1412, . URL `http://creckmodeling.chem.polimi.it/images/site/kinetic{_}mechanisms/version1412/POLIMI{_}PRF{_}PAH{_}LT{_}1412.CKI`.

[14] GRI. DRM19, . URL `http://combustion.berkeley.edu/drm/drm19.dat`.

[15] GRI. GRI3.0, . URL `http://combustion.berkeley.edu/gri-mech/version30/files30/grimech30.dat`.

[16] PoliMi. POLIMI_C1C3HT, . URL `http://creckmodeling.chem.polimi.it/index.php/menu-kinetics/menu-kinetics-detailed-mechanisms/menu-kinetics-c1-c3-mechanism`.

[17] PoliMi. POLIMI_PAH_HT, . URL `http://creckmodeling.chem.polimi.it/index.php/menu-kinetics/menu-kinetics-detailed-mechanisms/menu-kinetics-prf-pah-mechanism`.

[18] Benjamin J Isaac, Alessandro Parente, Chiara Galletti, Jeremy N Thornock, Philip J Smith, and Leonardo Tognotti. A Novel Methodology for Chemical Time Scale Evaluation with Detailed Chemical Reaction Kinetics. 2013.

[19] F.C. Christo and B.B. Dally. Modeling turbulent reacting jets issuing into a hot and diluted coflow. *Combustion and Flame*, 142(1-2):117–129, 2005. ISSN 00102180. doi: 10.1016/j.combustflame.2005.03.002.

[20] B. F. Magnussen. On the structure of turbulence and a generalized eddy dissipation concept for chemical reaction in turbulent flow, 1981.

[21] Bjørn F Magnussen. The Eddy Dissipation Concept. *Proceedings of ECCOMAS Thematic Conference on Computational Combustion , Lisbon , June 21-24 , 2005*, 2005.

[22] Bjorn F. Magnussen Ivar S. Ertesvag. The Eddy Dissipation Turbulence Energy Cascade Model. *Combustion Science and Technology*, 1999.

[23] R.S. Barlow and J.H. Frank. Effects of turbulence on species mass fractions in methane/air jet flames. *Symposium (International) on Combustion*, 27(1):1087–1095, 1998. ISSN 00820784. doi: 10.1016/S0082-0784(98)80510-9.

[24] R BARLOW, J FRANK, A KARPETIS, and J CHEN. Piloted methane/air jet flames: Transport effects and aspects of scalar structure. *Combustion and Flame*, 143(4):433–449, 2005. ISSN 00102180. doi: 10.1016/j.combustflame.2005.08.017.